

# Spontaneous emission and the operation of invisibility cloaks: Can the invisibility cloaks render objects invisible in quantum mechanic domain?

Mina Morshed Behbahani,<sup>1</sup> Ehsan Amooghoban,<sup>1,2,\*</sup> and Ali Mahdifar<sup>1,2</sup>

<sup>1</sup>*Department of Physics, Faculty of Basic Sciences,*

*Shahrekord University, P.O. Box 115, Shahrekord 88186-34141, Iran.*

<sup>2</sup>*Photonics Research Group, Shahrekord University, P.O. Box 115, Shahrekord 88186-34141, Iran.*

As a probe to explore the ability of invisibility cloaks to conceal objects in the quantum mechanics domain, we study the spontaneous emission rate of an excited two-level atom in the vicinity of an ideal invisibility cloaking. On this base, first, a canonical quantization scheme is presented for the electromagnetic field interacting with atomic systems in an anisotropic, inhomogeneous and absorbing magnetodielectric medium which can suitably be used for studying the influence of arbitrary invisibility cloak on the atomic radiative properties. The time dependence of the atomic subsystem is obtained in the Schrodinger picture. By introducing a modified set of the spherical wave vector functions, the Green tensor of the system is calculated via the continuous and discrete methods. In this formalism, the decay rate and as well the emission pattern of the aforementioned atom are computed analytically for both weak and strong coupling interaction, and then numerically calculations are done to demonstrate the performances of cloaking in the quantum mechanics domain. Special attention is paid to different possible orientations and locations of atomic system near the spherical invisibility cloaking. Results in the presence and the absence of the invisibility cloak are compared. We find that the cloak works very well far from its resonance frequency to conceal a macroscopic object, whereas at near the resonance frequency the object is more visible than the situation that the object is not covered by the cloak.

## I. INTRODUCTION

As a result of the implement of many intriguing features that have not yet been found in nature, metamaterial has attracted a great deal of attention in the field of optics. These features prepare new opportunities for realizing exotic phenomena such as invisibility devices [1]- [3], superlenses [4, 5], field rotators [6], optical analogues of black holes [7, 8], Schwarzschild space-time [21], wormholes [10] and the "Big Bang" and cosmological in ation [11, 12]. The theoretical basis for some of these phenomena is coordinate transformation, which stems from the formal invariance of Maxwells equations. This enable both physics and engineering societies to manipulate electromagnetic waves in almost any fashion. In this paper, we focus on the invisibility cloaking, and attempt to gain some physical insight regarding the quantum electrodynamics of this topic.

Based on a coordinate transformation, Pendry et al. first proposed an invisibility cloak, which can protect the cloaked object of arbitrary shape from electromagnetic radiation. The external observer got therefore unaware of the presence of the cloak and the object. This idea has been verified numerically by full-wave simulations [13] and experimentally by using metamaterial at the microwave frequency [3], and even at the optical frequencies [14]. However, these invisibility cloaks were encountered a serious limitation: they required extreme values of material properties and can only work within a narrow-band frequency. The first issue is circumvented

by using simplified constitutive parameters [3]. To overcome the bandwidth limitation, it was proposed carpet cloak to conceal an object that is placed under a bulging reflecting surface by imitating the reflection of a flat surface [15]. Such cloaks were experimentally demonstrated in both microwave [16, 17] and optical frequencies [18]-[20] using metamaterial structures with feature sizes in the centimeter to nanometer scale. It inevitably requires complicated nanofabrication processes which restrict the size of hiding objects in the visible frequencies to a few wavelengths. So, this carpet cloaking has not enabled to hide a large object at least as experimentally. Furthermore, the scattered waves are suffered a lateral shift, which makes the object to be detectable. To bypass these limitations, macroscopic invisibility cloaking has been introduced by using the birefringence property of a natural crystal such as calcite at broadband visible wavelengths [21, 22].

As mentioned above briefly, all researches on cloaking reported so far have been focused on the case in which the electromagnetic field is taken into account classically. However, the performances of cloaking in the quantum mechanics domain, which can be an important topic, have been rarely considered [23]. The question that naturally arises in this context is whether such invisibility cloaks work in the quantum mechanics domain as well as in the classical regime. The present paper is intended to respond to this question. Without loss the generality of our approach, we restrict our attention to the special case at Pendry cloaking which was relatively easy to be constructed, simulated and analyzed.

It is well known that the spontaneous decay of an atom is influenced by the geometry and the optical properties of the material body. We therefore expect that if an atom

---

\* Ehsan.amooghoban@sci.sku.ac.ir

is located near the ideal invisibility cloaking, the electromagnetic interaction between them will lead to drastically modification of the density of radiation modes and subsequently the spontaneously decay rate. In this sense, it is useful to look at the decay rate of an excited atom as a probe that allows us to examine the operation of this type of cloaks in the quantum mechanic regime. On this base, we study the spontaneous emission of an excited two-level atom and as well the spatial distribution of its radiation intensity as a function of the atomic transition frequency and the distance between the atom and the invisibility cloaking.

On one hand, the spontaneous emission is a phenomena which corresponds to the conventional framework of quantum electrodynamics. On the other hand, such invisibility cloak with position-dependent and anisotropic optical parameters was demonstrated for microwave frequencies by utilizing concentric layers of split-ring resonators. Due to the metallic nature of resonator structure, such invisibility cloaks are usually associated with a high loss factor and accompanied by a strong dispersion to fulfill causality. Therefore, a fully quantum mechanical treatment is needed to consider the dissipative and dispersive effects of the invisibility cloak along with their inhomogeneous and anisotropic features on the spontaneous emission rate.

There are two approaches to quantize the electromagnetic field in the presence of a dissipative and dispersive media, in general: canonical and phenomenological method. In this paper, we consider the rigorous canonical approach. For this purpose, as a lateral purpose of the present paper, we extend the canonical quantization scheme in [24]-[27] to a more general case that the medium is described in terms of a spatially varying and anisotropic permittivity and permeability, and as well the composed field-medium system interacting with atomic systems. This derivation helps us to gain a physical insight into the influence of arbitrary cloak on the atomic radiative properties.

The paper is organized as follows. In Sec. II we present a canonical quantization of the electromagnetic field interacting with charged particles in presence of an anisotropic, inhomogeneous and absorbing magnetodielectric medium. In Sec. III, the spontaneous emission rate of an excited atom near a spherical invisibility cloak is expressed in terms of the imaginary part of the classical Green tensor at the position of the atom. By expanding the Green tensor of system into a modified set of the spherical wave vector functions, the decay rate is computed analytically in both weak and strong coupling regime. As an application of this formalism, the numerical evaluations are performed for the spherical cloak whose material absorption and dispersion is of the Lorentz type. Then, we discuss the role of the orientation of the dipole moment of atomic system. In Sec. IV the spatial intensity of the spontaneously emitted light is calculated as functions of the atomic transition frequency and the distance between the atom and the hidden object

which is covered by the spherical invisibility cloaking. A summary and conclusions are presented in Sec. V. The derivation of the Green tensor via two methods, exact and discrete, is provided in Appendix A.

## II. CANONICAL QUANTIZATION OF ELECTROMAGNETIC FIELD

Our analysis of the spontaneous decay of an excited atom placed in vicinity of a Pendry cloaking is based on a generalization of a canonical scheme for quantization of the electromagnetic field in an isotropic magnetodielectrics medium developed in Refs [24]-[27]. We give only the bare essentials needed for an appreciation of the present paper.

Based on an inspiration of the microscopic Hopfield model [28], quantum electrodynamics in an inhomogeneous, anisotropic, dissipative and dispersive magnetodielectric medium can be accomplished by modeling the medium by two independent reservoirs comprised of a continuum of three dimensional harmonic oscillators. These two independent sets of harmonic oscillators are characterized by means of two harmonic oscillator fields  $\mathbf{X}_\omega$  and  $\mathbf{Y}_\omega$  which interact with the electric and the magnetic fields through a dipole interaction term. Hereby, we can describe the polarizability and the magnetizability characters of the magnetodielectric medium, as well as its dissipative behavior. Bearing these in mind, let us start with the total Lagrangian density of the system composed of the electromagnetic field, the external charged particles and the medium including the dissipative behavior

$$\mathcal{L} = \mathcal{L}_{\text{EM}} + \mathcal{L}_e + \mathcal{L}_m + \mathcal{L}_q + \mathcal{L}_{\text{int}}, \quad (1)$$

where the electromagnetic part  $\mathcal{L}_{\text{EM}}$  has the standard form  $\mathcal{L}_{\text{EM}} = \frac{1}{2}\epsilon_0 \mathbf{E}^2(\mathbf{r}, t) - \frac{1}{2\mu_0} \mathbf{B}^2(\mathbf{r}, t)$  that the electric field  $\mathbf{E} = -\partial \mathbf{A}/\partial t - \nabla \phi$  and magnetic field  $\mathbf{B} = \nabla \times \mathbf{A}$  are written in terms of the vector potential  $\mathbf{A}$  and scalar potential  $\phi$ . The electric and the magnetic parts of the material Lagrangian density  $\mathcal{L}_e$  and  $\mathcal{L}_m$ , which are modeled by a continuum of harmonic oscillators, are given by  $\frac{1}{2} \int_0^\infty d\omega \left[ \dot{\mathbf{X}}_\omega^2(\mathbf{r}) - \omega^2 \mathbf{X}_\omega^2(\mathbf{r}) \right]$  and  $\frac{1}{2} \int_0^\infty d\omega \left[ \dot{\mathbf{Y}}_\omega^2(\mathbf{r}) - \omega^2 \mathbf{Y}_\omega^2(\mathbf{r}) \right]$ , respectively. The polarization and magnetization fields of the medium in term of two harmonic oscillator fields  $\mathbf{X}_\omega$  and  $\mathbf{Y}_\omega$  are defined as

$$\mathbf{P}(\mathbf{r}, \omega) = \int_0^\infty d\omega \bar{g}_e(\mathbf{r}, \omega) \cdot \mathbf{X}_\omega(\mathbf{r}, \omega), \quad (2a)$$

$$\mathbf{M}(\mathbf{r}, \omega) = \int_0^\infty d\omega \bar{g}_m(\mathbf{r}, \omega) \cdot \mathbf{Y}_\omega(\mathbf{r}, \omega), \quad (2b)$$

where the interaction with the material is described via the coupling tensors,  $\bar{g}_e(\mathbf{r}, \omega)$  and  $\bar{g}_m(\mathbf{r}, \omega)$ , which are assumed to be analytic functions of  $\omega$  in the upper half plane. It is worth noting that the permittivity and the permeability of medium will be determined in term of

these coupling tensors. So, we take here the coupling tensor as a function of position to be the second order tensor, since the Pendry clocks under consideration are nothing but an inhomogeneous and anisotropic metamaterial.

The forth term in Eq. (1) is the Lagrangian density of free charged particles with particles mass  $m_\alpha$  and position  $\mathbf{r}_\alpha$ , which is written as

$$\mathcal{L}_q = \frac{1}{2} \sum_{\alpha} m_{\alpha} \dot{\mathbf{r}}_{\alpha}^2. \quad (3)$$

Finally,  $\mathcal{L}_{int}$  is the interaction Lagrangian density which includes the linear interaction between the medium and the charged particles with the electromagnetic field. It is found that such interaction is given by

$$\mathcal{L}_{int} = \mathbf{J}(\mathbf{r}_\alpha, t) \cdot \mathbf{A}(\mathbf{r}_\alpha, t) - \rho(\mathbf{r}_\alpha) \varphi(\mathbf{r}_\alpha) + \mathbf{P}(\mathbf{r}, t) \cdot \mathbf{E}(\mathbf{r}, t) + \nabla \times \mathbf{A}(\mathbf{r}, t) \cdot \mathbf{M}(\mathbf{r}, t) \quad (4)$$

where  $\mathbf{J}(\mathbf{r}_\alpha, t)$  is the current density of charged particles. An analysis of the Lagrangian density (1) shows that the scalar potential  $\phi$  does not appear. Therefore, the scalar potential is not a proper dynamical variable and the corresponding equation of motion can be treated as a constraint. It enables us to eliminate the scalar potential, and then get a reduced Lagrangian where only the vector potential  $\mathbf{A}$ , the material fields  $\mathbf{X}_\omega$  and  $\mathbf{Y}_\omega$ , and their time derivatives are appeared. To do this, we apply Euler-Lagrange equations to the scalar potential. It leads to

$$\begin{aligned} \varphi &= \varphi_A + \varphi_P \\ &= \frac{1}{4\pi\epsilon_0} \int d^3r' \frac{\rho_A(\mathbf{r}')}{|\mathbf{r} - \mathbf{r}'|} + \frac{1}{4\pi\epsilon_0} \int d^3r' \frac{\rho_P(\mathbf{r}')}{|\mathbf{r} - \mathbf{r}'|}, \end{aligned} \quad (5)$$

where  $\rho_A(\mathbf{r}) = \sum_{\alpha} \mathbf{e}_{\alpha} \delta(\mathbf{r} - \mathbf{r}_{\alpha})$  and  $\rho_P(\mathbf{r}) = -\nabla \cdot \mathbf{P}(\mathbf{r})$  are the charge density and polarization-charge density, respectively, and subsequently  $\varphi_A$  and  $\varphi_P$  are the corresponding scalar potentials arisen from these charge distributions. By substituting Eq.(5) into Lagrangian (1), the total Lagrangian can be recast into the reduced form

$$\begin{aligned} \mathcal{L} &= \frac{1}{2} \sum_{\alpha} m_{\alpha} \dot{\mathbf{r}}_{\alpha}^2 + \frac{1}{2} \epsilon_0 \dot{\mathbf{A}}^2(\mathbf{r}, t) - \frac{1}{2\mu_0} (\nabla \times \mathbf{A}(\mathbf{r}, t))^2 \\ &+ \frac{1}{2} \int_0^\infty d\omega \left\{ \dot{\mathbf{X}}_{\omega}^2(\mathbf{r}, t) - \omega^2 \mathbf{X}_{\omega}^2(\mathbf{r}, t) \right\} \\ &+ \frac{1}{2} \int_0^\infty d\omega \left\{ \dot{\mathbf{Y}}_{\omega}^2(\mathbf{r}, t) - \omega^2 \mathbf{Y}_{\omega}^2(\mathbf{r}, t) \right\} \\ &+ \sum_{\alpha} e_{\alpha} \dot{\mathbf{r}}_{\alpha} \cdot \mathbf{A}(\mathbf{r}_{\alpha}, t) + \mathbf{A} \cdot \dot{\mathbf{P}}(\mathbf{r}, t) + \mathbf{M} \cdot \nabla \times \mathbf{A}(\mathbf{r}, t) \\ &- W_{coul}, \end{aligned} \quad (6)$$

where  $W_{coul}$  is Coulomb energy of the charged particles, the polarization-charge and their interactions which in term of  $\varphi_A$  and  $\varphi_P$  is defined as

$$\begin{aligned} W_{coul} &= \frac{1}{2} \int d^3r \rho_A(\mathbf{r}) \varphi_A(\mathbf{r}) + \int d^3r \rho_P(\mathbf{r}) \varphi_P(\mathbf{r}) \\ &+ \frac{1}{2} \int d^3r \rho_P(\mathbf{r}) \varphi_P(\mathbf{r}). \end{aligned} \quad (7)$$

The Lagrangian (6) can now be used to obtain the corresponding canonical conjugate variables for the fields

$$-\epsilon_0 \mathbf{E}^{\perp}(\mathbf{r}, t) = \frac{\delta L}{\delta \dot{\mathbf{A}}(\mathbf{r}, t)} = \epsilon_0 \dot{\mathbf{A}}(\mathbf{r}, t), \quad (8a)$$

$$\mathbf{Q}_{\omega}(\mathbf{r}, t) = \frac{\delta L}{\delta \dot{\mathbf{X}}_{\omega}(\mathbf{r}, t)} = \bar{g}_e(\mathbf{r}, \omega) \mathbf{A}(\mathbf{r}, t) + \dot{\mathbf{X}}_{\omega}(\mathbf{r}, t), \quad (8b)$$

$$\mathbf{\Pi}_{\omega}(\mathbf{r}, t) = \frac{\delta L}{\delta \dot{\mathbf{Y}}_{\omega}(\mathbf{r}, t)} = \dot{\mathbf{Y}}_{\omega}(\mathbf{r}, t), \quad (8c)$$

$$\mathbf{p}_{\alpha}(\mathbf{r}_{\alpha}, t) = \frac{\partial L}{\partial \dot{\mathbf{r}}_{\alpha}} = m_{\alpha} \dot{\mathbf{r}}_{\alpha} + e_{\alpha} \mathbf{A}(\mathbf{r}_{\alpha}, t). \quad (8d)$$

Now, the transition from the classic to the quantum domain can be accomplished in a standard fashion by applying commutation relation on the variables and their corresponding conjugates. For the electromagnetic field, we have

$$\left[ \hat{A}(r, t), -\epsilon_0 \hat{E}^{\perp}(r', t) \right] = i\hbar \delta^{\perp}(r - r'), \quad (9)$$

and for the material fields and the dynamical variable of charged particles

$$\left[ \hat{X}_{\omega}(r, t), \hat{Q}_{\omega'}(r', t) \right] = i\hbar \delta(r - r') \delta(\omega - \omega'), \quad (10a)$$

$$\left[ \hat{Y}_{\omega}(r, t), \mathbf{\Pi}_{\omega'}(r', t) \right] = i\hbar \delta(r - r') \delta(\omega - \omega'), \quad (10b)$$

$$[q_{\alpha}, \hat{p}_{\beta}(r, t)] = i\hbar \delta_{\alpha\beta}. \quad (10c)$$

By applying the Lagrangian (1) and the expressions for canonical conjugate variables in (8), we can form the Hamiltonian density as,

$$\begin{aligned} \mathcal{H} &= \sum_{\alpha} \frac{1}{2m_{\alpha}} [\mathbf{p}_{\alpha}(\mathbf{r}_{\alpha}, t) - e_{\alpha} \mathbf{A}(\mathbf{r}_{\alpha}, t)]^2 + \frac{1}{2} \epsilon_0 \mathbf{E}^{\perp 2}(\mathbf{r}, t) \\ &+ \frac{\mathbf{B}^2(\mathbf{r}, t)}{2\mu_0} + \frac{1}{2} \int_0^\infty d\omega \left\{ \mathbf{Q}_{\omega}(\mathbf{r}, t) + \omega^2 \dot{\mathbf{X}}_{\omega}^2(\mathbf{r}, t) \right\} \\ &+ \frac{1}{2} \int_0^\infty d\omega \left\{ \mathbf{\Pi}_{\omega}(\mathbf{r}, t) + \omega^2 \dot{\mathbf{Y}}_{\omega}^2(\mathbf{r}, t) \right\} \\ &- \nabla \times \mathbf{A}(\mathbf{r}, t) \cdot \mathbf{M}(\mathbf{r}, t) - \dot{\mathbf{P}}(\mathbf{r}, t) \cdot \mathbf{A}(\mathbf{r}, t) \\ &- \frac{1}{2} \int_0^\infty d\omega (\bar{g}_e(\mathbf{r}, \omega) \cdot \mathbf{A}(\mathbf{r}, t))^2 + W_{coul}. \end{aligned} \quad (11)$$

By using the Hamiltonian density (11) and recalling the commutation relations (9) and (10), it is straightforward to prove that the Heisenberg equations for the vector potential, the transverse electric field and the particle coordinates yield the correct Maxwell equations and the Newtonian equation of motion in the quantum domain. Let us begin with the Heisenberg equations for the vector potential and the transverse electric field. Thus, the time derivative of  $\mathbf{A}$  and  $\mathbf{E}^{\perp}$  in a straightforward manner is given by

$$\dot{\mathbf{A}}(\mathbf{r}, t) = \frac{1}{i\hbar} [\mathbf{A}(\mathbf{r}, t), \mathcal{H}] = -\mathbf{E}^{\perp}(\mathbf{r}, t), \quad (12a)$$

$$\begin{aligned} \epsilon_0 \dot{\mathbf{E}}^{\perp}(\mathbf{r}, t) &= \frac{1}{i\hbar} [\epsilon_0 \mathbf{E}^{\perp}(\mathbf{r}, t), \mathcal{H}] = \frac{\nabla \times \nabla \times \mathbf{A}(\mathbf{r}, t)}{\mu_0} \\ &- \nabla \times \mathbf{M}(\mathbf{r}, t) - \dot{\mathbf{P}}^{\perp}(\mathbf{r}, t) - \mathbf{J}^{\perp}(\mathbf{r}, t) \end{aligned} \quad (12b)$$

By using the constitutive equations of the displacement field  $\mathbf{D}^\perp = \varepsilon_0 \mathbf{E}^\perp + \mathbf{P}^\perp$  and the magnetic field strength  $\mathbf{H} = \mathbf{B}/\mu_0 - \mathbf{M}$ , Eqs.(12) lead to  $\dot{\mathbf{D}}^\perp(\mathbf{r}, t) = \nabla \times \mathbf{H}^\perp(\mathbf{r}, t) - \mathbf{J}^\perp(\mathbf{r}, t)$  and  $\dot{\mathbf{B}}(\mathbf{r}, t) = -\nabla \times \mathbf{E}(\mathbf{r}, t)$  as expected, where  $\mathbf{D}^\perp$  is the transverse displacement field and  $\mathbf{J}^\perp$  is transverse component of current density. In the presence of charged particles, the longitudinal components of electric and displacement fields can be written respectively as

$$\mathbf{E}^\parallel(\mathbf{r}, t) = -\frac{\mathbf{P}^\parallel(\mathbf{r}, t)}{\varepsilon_0} - \nabla\varphi_A, \quad (13a)$$

$$\mathbf{D}^\parallel(\mathbf{r}, t) = \varepsilon_0 \mathbf{E}^\parallel(\mathbf{r}, t) + \mathbf{P}^\parallel(\mathbf{r}, t) = -\varepsilon_0 \nabla\varphi_A. \quad (13b)$$

The Heisenberg equation of the charged particles in presence of  $\mathbf{E}$  and  $\mathbf{B}$  leads to the quantum mechanical version of Lorentz force, namely,

$$m\ddot{\mathbf{r}}_\alpha = \frac{1}{i\hbar} [m\dot{\mathbf{r}}_\alpha, \mathcal{H}] = e_\alpha \mathbf{E}(\mathbf{r}_\alpha, t) + e_\alpha \dot{\mathbf{r}}_\alpha \times \mathbf{B}(\mathbf{r}_\alpha, t). \quad (14)$$

Calculations analogous to those of (12) give the following Heisenberg equations for the dynamical variables  $\mathbf{X}_\omega$  and  $\mathbf{Y}_\omega$ , respectively, as

$$\ddot{\mathbf{X}}_\omega(\mathbf{r}, t) = -\omega^2 \mathbf{X}_\omega(\mathbf{r}, t) + \bar{g}_e(\mathbf{r}, t) \cdot \mathbf{E}(\mathbf{r}, t), \quad (15a)$$

$$\ddot{\mathbf{Y}}_\omega(\mathbf{r}, t) = -\omega^2 \mathbf{Y}_\omega(\mathbf{r}, t) + \bar{g}_m(\mathbf{r}, t) \cdot \mathbf{B}(\mathbf{r}, t). \quad (15b)$$

The formal solution of Eq.(15a) is obtained as

$$\begin{aligned} \mathbf{X}_\omega(\mathbf{r}, t) = & \left( \dot{\mathbf{X}}_\omega(\mathbf{r}, 0) \frac{\sin \omega t}{\omega} + \mathbf{X}_\omega(\mathbf{r}, 0) \cos \omega t \right) \\ & + \bar{g}_e(\mathbf{r}, \omega) \cdot \int_0^t dt' \mathbf{E}(\mathbf{r}, t') \frac{\sin \omega(t-t')}{\omega}. \end{aligned} \quad (16)$$

A similar relation also holds for  $\mathbf{Y}_\omega(\mathbf{r}, t)$ . To facilitate the calculations, let us introduce the following annihilation operators:

$$\mathbf{f}_e(\mathbf{r}, \omega, t) = \frac{1}{\sqrt{2\hbar\omega}} [-i\omega \mathbf{X}_\omega(\mathbf{r}, t) + \mathbf{Q}_\omega(\mathbf{r}, t)], \quad (17a)$$

$$\mathbf{f}_m(\mathbf{r}, \omega, t) = \frac{1}{\sqrt{2\hbar\omega}} [\omega \mathbf{Y}_\omega(\mathbf{r}, t) + i\mathbf{\Pi}_\omega(\mathbf{r}, t)], \quad (17b)$$

where  $\mathbf{f}_e$  and  $\mathbf{f}_m$  denote two independent infinite sets of bosonic operators, which associated with the electric and magnetic excitations of the system. By making use of Eqs. (10a) and (10b), it is easily seen that the bosonic operators have the commutation relations of the form

$$[\mathbf{f}_{ej}(\mathbf{r}, \omega, t), \mathbf{f}_{ej'}^\dagger(\mathbf{r}', \omega', t)] = \delta_{jj'} \delta(\omega - \omega') \delta(\mathbf{r} - \mathbf{r}'), \quad (18a)$$

$$[\mathbf{f}_{mj}(\mathbf{r}, \omega, t), \mathbf{f}_{mj'}^\dagger(\mathbf{r}', \omega', t)] = \delta_{jj'} \delta(\omega - \omega') \delta(\mathbf{r} - \mathbf{r}'). \quad (18b)$$

We can now invert Eq. (17) to obtain the material field  $\mathbf{X}_\omega$  and  $\mathbf{Y}_\omega$  in term of the bosonic operators  $\mathbf{f}_e$  and  $\mathbf{f}_m$ . With this in mind, the polarization and magnetization

fields of the medium (2) in term of the bosonic operators are written as

$$\mathbf{P}(\mathbf{r}, t) = \varepsilon_0 \int_0^\infty dt' \bar{\chi}_e(\mathbf{r}, t-t') \cdot \mathbf{E}(\mathbf{r}, t') + \mathbf{P}^N(\mathbf{r}, t), \quad (19a)$$

$$\mathbf{M}(\mathbf{r}, t) = \mu_0^{-1} \int_0^\infty dt' \bar{\chi}_m(\mathbf{r}, t-t') \cdot \mathbf{B}(\mathbf{r}, t') + \mathbf{M}^N(\mathbf{r}, t), \quad (19b)$$

where electric and magnetic susceptibilities tensors of the medium are respectively defined as

$$\bar{\chi}_e(\mathbf{r}, t) = \Theta(t) \varepsilon_0^{-1} \int_0^\infty d\omega \bar{g}_e^t \cdot \bar{g}_e(\mathbf{r}, \omega) \frac{\sin \omega t}{\omega}, \quad (20a)$$

$$\bar{\chi}_m(\mathbf{r}, t) = \Theta(t) \mu_0 \int_0^\infty d\omega \bar{g}_m^t \cdot \bar{g}_m(\mathbf{r}, \omega) \frac{\sin \omega t}{\omega}. \quad (20b)$$

Here, the superscript  $t$  indicates the transpose of a tensor.

Let  $\bar{\chi}_e(\mathbf{r}, \omega)$  and  $\bar{\chi}_m(\mathbf{r}, \omega)$ , respectively, be the electric and the magnetic susceptibilities tensors in frequency space. Then the electric permittivity and the magnetic permeability tensors of the medium in term of the susceptibilities tensors are written as  $\bar{\varepsilon}(\mathbf{r}, \omega) = \bar{\mathbf{I}} + \bar{\chi}_e(\mathbf{r}, \omega)$  and  $\bar{\mu}^{-1}(\mathbf{r}, \omega) = \bar{\mathbf{I}} - \bar{\chi}_m(\mathbf{r}, \omega)$ , where  $\bar{\mathbf{I}}$  is the identity tensor. These are complex tensors of frequency which their real and imaginary parts satisfy Kramers-Kronig relations and their dependence on coupling tensors,  $\bar{g}_e$  and  $\bar{g}_m$ , are given through the susceptibilities tensors as:

$$\bar{\chi}_e(\mathbf{r}, \omega) = \varepsilon_0^{-1} \int_0^\infty d\omega' \frac{\bar{g}_e^t \cdot \bar{g}_e(\mathbf{r}, \omega')}{\omega'^2 - \omega^2 + i0^+}, \quad (21a)$$

$$\bar{\chi}_m(\mathbf{r}, \omega) = \mu_0 \int_0^\infty d\omega' \frac{\bar{g}_m^t \cdot \bar{g}_m(\mathbf{r}, \omega')}{\omega'^2 - \omega^2 + i0^+}. \quad (21b)$$

Given the electric permittivity and the magnetic permeability tensors of medium, we can inverse the relations (21) and obtain the coupling tensors in term of these response tensors. Therefore, we find

$$\bar{g}_e^t \cdot \bar{g}_e(\mathbf{r}, \omega) = \frac{2\varepsilon_0\omega}{\pi} \text{Im} [\bar{\varepsilon}(\mathbf{r}, \omega)], \quad (22a)$$

$$\bar{g}_m^t \cdot \bar{g}_m(\mathbf{r}, \omega) = -\frac{2\omega}{\pi\mu_0} \text{Im} [\bar{\mu}^{-1}(\mathbf{r}, \omega)]. \quad (22b)$$

The fields  $\mathbf{P}^N$  and  $\mathbf{M}^N$  in Eqs. (19) are, respectively, the noise polarization and the noise magnetization operators which associated to the dissipation effects within medium. As in the phenomenological method, we can separate the positive and negative parts of fields, like  $\mathbf{P}^N = \mathbf{P}^{N(+)} + \mathbf{P}^{N(-)}$ , where  $\mathbf{P}^{N(+)}$  is the conjugate of the negative part (analogously for  $\mathbf{M}^{N(+)}$ ) and yields

$$\mathbf{P}^{N(+)}(\mathbf{r}, t) = i \int_0^\infty d\omega \sqrt{\frac{\hbar}{2\omega}} \bar{g}_e(\mathbf{r}, \omega) \cdot \mathbf{f}_e(\mathbf{r}, \omega, 0) e^{-i\omega t}, \quad (23a)$$

$$\mathbf{M}^{N(+)}(\mathbf{r}, t) = \int_0^\infty d\omega \sqrt{\frac{\hbar}{2\omega}} \bar{g}_m(\mathbf{r}, \omega) \cdot \mathbf{f}_m(\mathbf{r}, \omega, 0) e^{-i\omega t}, \quad (23b)$$

By taking the time derivative of Maxwell's equations Eq. (12b) and using Eq. (19), we obtain the frequency-domain wave equation for the positive-frequency part of the vector potential as,

$$\begin{aligned} \nabla \times \bar{\mu}^{-1} \nabla \times \mathbf{E}^{(+)}(\mathbf{r}, \omega) - \frac{\omega^2}{c^2} \bar{\varepsilon}(\mathbf{r}, \omega) \mathbf{E}^{(+)}(\mathbf{r}, \omega) \\ = \mu_0 \omega^2 \mathbf{P}^{N(+)}(\mathbf{r}, \omega) + i\mu_0 \omega \nabla \times \mathbf{M}^{N(+)}(\mathbf{r}, \omega). \end{aligned} \quad (24)$$

The formal solution of the above equation may be obtained through finding an appropriate Green tensor. We thereby arrive at the following expression for the electric field

$$\begin{aligned} \mathbf{E}^{(+)}(\mathbf{r}, t) = (i\omega\mu_0) \int_0^\infty d\omega \int d^3r' \bar{\mathbf{G}}(\mathbf{r}, \mathbf{r}', \omega) \cdot \\ \left[ -i\omega \mathbf{P}^{N(+)}(\mathbf{r}', \omega) + \nabla \times \mathbf{M}^{N(+)}(\mathbf{r}', \omega) \right] e^{-i\omega t}, \end{aligned} \quad (25)$$

where  $\bar{\mathbf{G}}(\mathbf{r}, \mathbf{r}', \omega)$  is the classical Green tensor that satisfying the inhomogeneous Helmholtz equation with the space- and frequency-dependent complex permittivity and permeability of medium,

$$\begin{aligned} \nabla \times \left[ \bar{\mu}^{-1}(\mathbf{r}, \omega) \nabla \times \bar{\mathbf{G}}(\mathbf{r}, \mathbf{r}', \omega) \right] - \\ \frac{\omega^2 \bar{\varepsilon}(\mathbf{r}, \omega)}{c^2} \bar{\mathbf{G}}(\mathbf{r}, \mathbf{r}', \omega) = \delta^3(\mathbf{r} - \mathbf{r}') \bar{\mathbf{I}}, \end{aligned} \quad (26)$$

The set of Eqs. (23), (24), and (25) together with the commutation relations (12), provide us with the electromagnetic field quantization in an anisotropic, dissipative and dispersive magnetodielectric medium. It is easily seen that these relations are the same relations which were obtained via the phenomenological quantization method [29]- [33]. Thus, based on a rigorous quantization scheme, we arrive at the identical results.

### III. SPONTANEOUS DECAY OF AN EXCITED TWO-LEVEL ATOM

#### A. The model

Let us consider an excited two-level atom with transition frequency  $\omega_A$  and the dipole moment  $d_A$  placed at the point  $\mathbf{r}_A$  in the vacuum near an ideal invisibility cloaking. To simplify the treatment of the problem, we consider a spherical hidden object which is covered by an invisibility spherical shell. Furthermore, with regard to the symmetry of this cloak, we assume that the atom located on  $z$  axis. Our approach can be simply extended to other type of cloaks and other locations. In this case, the cloak in the annular region  $a < r < b$  is a kind of rotationally uniaxial media characterized by [1]

$$\bar{\varepsilon}(\mathbf{r}, \omega) = [(\varepsilon_r - \varepsilon_t)] \hat{r}\hat{r} + \varepsilon_t \bar{\mathbf{I}}, \quad (27)$$

$$\bar{\mu}(\mathbf{r}, \omega) = [(\mu_r - \mu_t)] \hat{r}\hat{r} + \mu_t \bar{\mathbf{I}}, \quad (28)$$

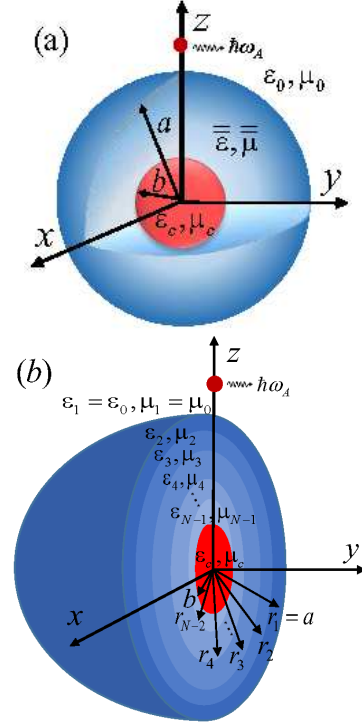


FIG. 1. (a) The schematic of a spherical invisibility cloak with the distribution of the material parameters which are given by Eq. (29). The cloak shell has inner and outer radius of  $b$  and  $a$ , respectively, and in the central region,  $r < b$ , is a homogeneous and isotropic material with the electric permittivity and the magnetic permeability function  $\varepsilon_c$  and  $\mu_c$  as an object should be hidden. The atom is placed at the distance  $r$  from the center of the cloak. Here, the media outside the cloak is free space. (b) The spherical invisibility cloak in part (a) is modeled by a large number of concentric layers with identical thickness.

where  $\bar{\mathbf{I}} = \hat{r}\hat{r} + \hat{\theta}\hat{\theta} + \hat{\phi}\hat{\phi}$  is the unit dyad, the subscripts  $r$  and  $t$  denote the parameters along radial  $\hat{r}$  and tangential direction  $\hat{\theta}$  or  $\hat{\phi}$ , respectively, and the permittivity and permeability tensor components for the cloak shell are given by

$$\varepsilon_t(\omega) = \mu_t(\omega) = \frac{b}{b-a} \kappa_L(\omega), \quad (29a)$$

$$\varepsilon_r(\mathbf{r}, \omega) = \mu_r(\mathbf{r}, \omega) = \frac{b}{b-a} \left( \frac{(r-a)^2}{r^2} \right) \kappa_L(\omega). \quad (29b)$$

Here,  $b$  is the inner radius (radius of hidden object) and  $a$  is the outer radius of the cloaking shell [see Fig. 1(a)]. As mentioned before in the introduction, to achieve above material parameters in experimental, the most of the cloak device are constructed with metamaterials consisting of resonating structures. This structure inevitably shows high loss and dispersion. For this purpose, we adopt a single-resonance Lorentz models for both the permittivity and permeability [34]. Thus, the permittivity and permeability tensor components of the cloak have been multiplied by a lorentzian factor,  $\kappa_L(\omega) =$

$\left(1 + \frac{\omega_p^2}{\omega_0^2 - \omega^2 - i\gamma\omega}\right)$ , to consider the material absorption and dispersion of metamaterial structures. Here,  $\omega_p$  and  $\omega_0$  are respectively the plasma frequency and the resonant frequency and  $\gamma$  is the absorption coefficient of the cloaking. Without loss of generality, we assume a homogeneous and isotropic object as a hidden object placed in the central region  $r < b$  with the material parameters  $\epsilon_c = \mu_c = \alpha\kappa_L(\omega)$  where  $\alpha$  is a constant.

The results obtained in the previous section can now be used to study the spontaneous emission of an excited two-level atom near such cloaked object. By inserting Eqs. (23) and (25) into (11), the Hamiltonian of the whole system under the electric-dipole approximation and the rotating wave approximation is recast to the following convenient form (refer to [24])

$$\hat{H} = \sum_{\lambda=e,m} \int d^3r \int_0^\infty d\omega \hbar\omega \hat{\mathbf{f}}_\lambda^\dagger(\mathbf{r}, \omega) \cdot \hat{\mathbf{f}}_\lambda(\mathbf{r}, \omega) + \hbar\omega_A \hat{\sigma}^\dagger \hat{\sigma} - \left[ \hat{\sigma}^\dagger \mathbf{d}_A \cdot \int_0^\infty d\omega \hat{\mathbf{E}}^{(+)}(\mathbf{r}_A, \omega) + \text{H.c.} \right] \quad (30)$$

Here,  $\hat{\sigma} = |l\rangle\langle u|$  and  $\hat{\sigma}^\dagger = |u\rangle\langle l|$  are respectively the atomic lowering and raising operators where  $|u\rangle$  ( $|l\rangle$ ) is the upper (lower) state of the atom whose energy is  $\hbar\omega_A$  (zero). Furthermore,  $\mathbf{d}_A$  is transition dipole moment which defined as  $\mathbf{d}_A = \langle l|\hat{\mathbf{d}}_A|u\rangle = \langle u|\hat{\mathbf{d}}_A|l\rangle$ . Since the spontaneous decay of an initially excited atom is studied here, the state of the whole of system at time  $t$  can be expanded into the ground and excited states of the composite system including electromagnetic field and the cloak,  $|\{0\}\rangle$  and  $|\mathbf{1}_\lambda(\mathbf{r}, \omega)\rangle$ , and the unperturbed atomic states as

$$|\psi(t)\rangle = C_u(t) e^{-i\tilde{\omega}_A t} |\{0\}\rangle |u\rangle + \sum_{\lambda=e,m} \int d^3r \int_0^\infty d\omega e^{-i\omega t} \mathbf{C}_{\lambda l}(\mathbf{r}, \omega, t) \cdot |\mathbf{1}_\lambda(\mathbf{r}, \omega)\rangle |l\rangle, \quad (31)$$

The population probability amplitudes of the upper and lower states of the whole system,  $C_u$  and  $C_{\lambda l}$ , can be easily calculated from the Schrödinger equation. In the case of  $C_u(t)$ , by making use of the Green tensor integral relationship that was proven in [31, 33], and inserting the initial conditions  $C_u(0) = 1$  and  $C_\lambda(\mathbf{r}, \omega, 0) = 0$ , the following time evolution is yield:

$$\dot{C}_u(t) = -i\delta\omega C_u(t) + \int_0^t dt' K(t-t') C_u(t'), \quad (32)$$

where the kernel function  $K(t-t')$  is determined by the Green tensor of the system in the position of the atom

$$K(t-t') = -\frac{1}{\hbar\pi\epsilon_0} \int_0^\infty d\omega \frac{\omega^2}{c^2} e^{-i(\omega-\tilde{\omega}_A)(t-t')} \times \mathbf{d}_A \cdot \text{Im}[\bar{\bar{G}}(\mathbf{r}_A, \mathbf{d}_A, \omega_A)] \cdot \mathbf{d}_A, \quad (33)$$

in which  $\tilde{\omega}_A = \omega_A - \delta\omega$  is the shifted transition frequency of the atom in the presence of the cloak and  $\delta\omega$  is the

Lamb shift. It is easily seen that the coupled integro-differential equation (32) cannot be solved analytically. But, we can gain a physical insight into the spontaneous emission process of the atomic system near the cloak on base of the analytical solutions. So, we concentrate our attention to the limiting cases of weak and strong atom-field coupling.

## B. Weak and strong coupling regimes

Let us first consider the weak coupling where the atom is only slightly perturbed by the vacuum fields, then the Markov approximation applies. In this regime, the coefficient  $C_u(t')$  in Eq. (32) can be replaced by  $C_u(t)$  and the time integral  $\int_0^t dt' e^{-i(\omega-\tilde{\omega}_A)(t-t')}$  in Eq.(33) can be approximated by the zeta function  $\xi(\tilde{\omega}_A - \omega)$  where  $\xi(x) = \pi\delta(x) + iP(\frac{1}{x})$ . By applying these approximations, the probability amplitude  $C_u(t')$  is written as the form

$$C_u(t) = \exp\left[\left(-\frac{1}{2}\Gamma + i\delta\omega\right)t\right], \quad (34)$$

where the Lamb shift  $\delta\omega$  and the decay rate  $\Gamma$  are given respectively as

$$\delta\omega = \frac{1}{\hbar\pi\epsilon_0} P \int_0^\infty d\omega \frac{\omega^2}{c^2} \frac{\mathbf{d}_A \cdot \text{Im}\bar{\bar{G}}(\mathbf{r}_A, \mathbf{r}_A, \omega) \cdot \mathbf{d}_A}{\omega - \tilde{\omega}_A}, \quad (35a)$$

$$\Gamma = \frac{2\tilde{\omega}_A^2}{\hbar\epsilon_0 c^2} \mathbf{d}_A \cdot \text{Im}\bar{\bar{G}}(\mathbf{r}_A, \mathbf{r}_A, \tilde{\omega}_A) \cdot \mathbf{d}_A. \quad (35b)$$

It is obviously seen that the effect of cloak and their properties are contained in the Green tensor. Therefore, in order to calculate the spontaneous emission rate of the excited atom, we first need to compute the Green tensor of the system.

As seen from Eq. (29), the cloak shell requires the material parameters with radius-dependent and anisotropic characteristics. At the first glance, it seems that the calculation of the Green tensor of such system, which is needed for substitution in Eq. (35b), is impossible. However, in the special case in which the cloak has a symmetric geometry shape such as the spherical cloak, the evaluation of the Green tensor, though lengthy, is rather straightforward. We call this Green tensor extraction *exact* method against another one which is approximately called *discrete* method. The latter one is important at least from one aspect: It offers the possibility of realizing such cloak by layered structures in experimental [3], since the evaluation of the Green tensor is done by a discrete model of layered structure.

Similar to the practical realization of an anisotropic and inhomogeneous cylindrical cloak by concentric layered structure consisting of anisotropic structure [3], we can imagine a layered structure of *homogeneous* and *anisotropic* materials to mimic the ideal cloak by enforcing the tangential components of the permittivity and

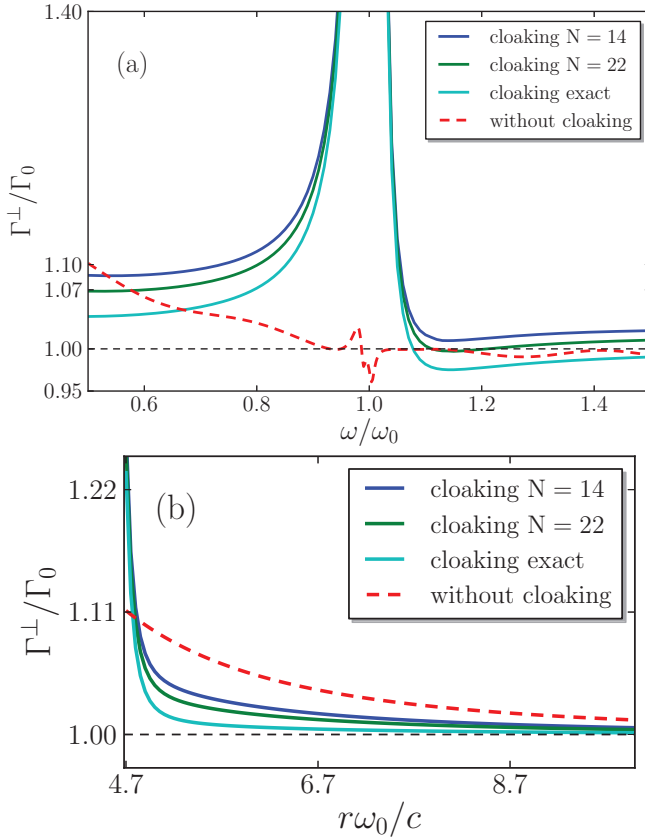


FIG. 2. The vertical spontaneous emission rate (41a) as a function of (a) the dimensionless frequency  $\omega_A/\omega_0$  and (b) the dimensionless distance  $r\omega_0/c$ . The material absorption and dispersion of the central hidden object and the cloak are described by the Lorentz model with parameters  $\omega_p = 0.01\omega_0$  and  $\gamma = 0.01\omega_0$ . The inner and outer radius of the cloak shell have been chosen  $b = 3c/\omega_0$  and  $a = 4.5c/\omega_0$ , respectively, and the excited two-level atom placed at  $r_A = 4.7c/\omega_0$ . For comparison, the spontaneous decay in free space is shown with black dashed line.

the permeability of different layers to vary with the radius according to Eq. (29). The cloak that is modeled in this manner [see Fig.1(b)], is an example of a spherically layered magnetodielectric medium for which its dyadic Green function is known [35, 37]. The details of these calculation are omitted here for the sake of brevity. The complete descriptions of both methods are given in Appendix A.

Of course, a cloaking structure was proposed in [38, 39], that does not require metamaterials to realize the anisotropy or inhomogeneity of the material parameters. This allows us to realize the cloak through natural materials by using a layered structure of alternating *homogeneous* and *isotropic* materials. We do not consider this proposed method here.

Now, we assume that the imaginary part of the Green tensor in the resonance region of atom-field coupling has a Lorentzian shape with the central frequency  $\omega_c$  and the half width at half maximum  $\delta\omega_c$ . Unlike to the weak cou-

pling, the zeta function no longer act as the  $\delta$  function. In this case, the frequency integral in Eq. (33) can be done by expanding the limit of integration to  $\pm\infty$  which leads to [32]

$$\bar{K}(t-t') = -\frac{1}{2}\Gamma\delta\omega_c e^{-i(\omega_c-\omega_A)(t-t')} e^{-\delta\omega_c|t-t'|}. \quad (36)$$

By substituting the above expression into Eq. (32) and making the differentiation of both sides of the resulting equation over time, one arrives at a second order homogeneous differential equation

$$\ddot{C}_u(t) + [i(\omega_c - \omega_A) + \delta\omega_c]\dot{C}_u(t) + (\Omega/2)^2 C_u(t) = 0, \quad (37)$$

where  $\Omega = \sqrt{2\Gamma\delta\omega_c}$ . This is in the form of the damped harmonic oscillator equation with the formal solution given for  $\omega_A \approx \omega_c$  by

$$C_u(t) = \frac{1}{2} \left( 1 + \frac{\delta\omega_c}{\sqrt{\delta\omega_c^2 - \Omega^2}} \right) e^{(-\delta\omega_c + \sqrt{\delta\omega_c^2 - \Omega^2})\frac{t}{2}} + \frac{1}{2} \left( 1 - \frac{\delta\omega_c}{\sqrt{\delta\omega_c^2 - \Omega^2}} \right) e^{(-\delta\omega_c - \sqrt{\delta\omega_c^2 - \Omega^2})\frac{t}{2}}. \quad (38)$$

It is seen that when  $\Omega \gg \delta\omega_c$ , the decay probability amplitude of the upper atomic state shows the well-known phenomenon of damped Rabi oscillations

$$C_u(t) = e^{-\frac{\delta\omega_c}{2}t} \cos(\Omega t/2). \quad (39)$$

This is the principal signature of strong atom-field coupling. In the opposite case, when  $\Omega \ll \delta\omega_c$ , we recover the weak coupling result (34) which obtained within the Markovian approximation.

### C. Analytical and numerical results

Equation (35b) can now be applied to the atom which its atomic dipole moment may be perpendicular to the interface along the  $z$  axis, and/or parallel to the interface along the  $y$  axis. We denote the former case by the superscript  $\perp$  and the latter one by the superscript  $\parallel$ . With the Greens tensor in hand given in [Appendix A] and use of the symmetry of our system, the scattering part of the Green tensor for the two special cases of radial and tangential direction are simplified as follows:

$$\bar{G}_s^{(11)}(\mathbf{r}_A, \mathbf{r}_A, \omega) = \frac{ik_1\mu_1}{4\pi} \sum_{n=0}^{\infty} n(n+1)(2n+1) \times B_N^{11} \left( \frac{z_n^{(1)}(kr)}{kr} \right)^2, \quad (40a)$$

$$\bar{G}_s^{(11)}(\mathbf{r}_A, \mathbf{r}_A, \omega) = \frac{ik_1\mu_1}{8\pi} \sum_{n=0}^{\infty} (2n+1) B_M^{11} \left( z_n^{(1)}(kr) \right)^2 + B_N^{11} \left( \frac{1}{kr} \frac{d[rz_n^{(1)}(kr)]}{dr} \right)^2. \quad (40b)$$

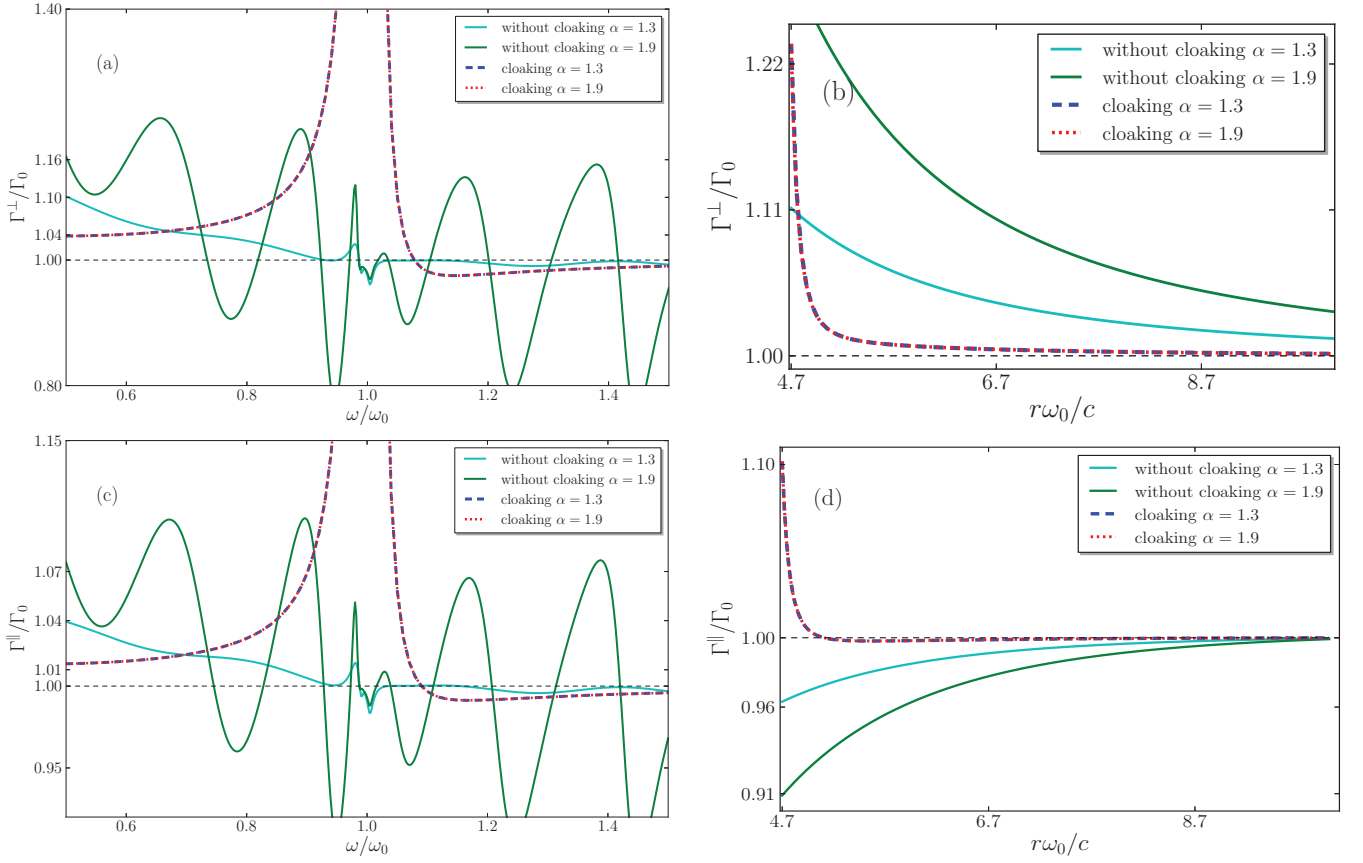


FIG. 3. The vertical spontaneous emission rate (41a) as a function of (a) the dimensionless frequency  $\omega_A/\omega_0$  and (b) the dimensionless distance  $r\omega_0/c$ . Panels (c) and (d) are the same as panels (a) and (b) but for the case that the atomic dipole moment is parallel to the cloak shell and the spontaneous emission rate is calculated by Eq. (41b). Here, the parameters are identical to those used in Fig. 2.

It is worth noting that in the above derivation of Eq. (40) seams only one of the electromagnetic Green tensors of our system which have been obtained in Eqs. (A16a) and (A24) to be used here. In fact, the exact Green tensor (A16a) has exactly the same form as the discrete Green tensor (A24) for  $f = 1$  with one exception for the coefficients  $B_{N,M}^{11}$  which given by Eqs. (A18) and (A29), respectively. This follows from the assumption that the field point and source point in our case are located out of the cloak.

By substituting the expressions above into Eq. (35b), we arrive at the following formulas for the spontaneous decay rate of the aforementioned atom at arbitrary posi-

tion

$$\frac{\Gamma^\perp}{\Gamma_0} = 1 + \frac{6\pi}{\omega} \text{Im} \left[ \frac{ik_1\mu_1}{4\pi} \sum_{n=0}^{\infty} n(n+1)(2n+1) \times B_N^{11} \left( \frac{z_n^{(1)}(kr)}{kr} \right)^2 \right], \quad (41a)$$

$$\frac{\Gamma^\parallel}{\Gamma_0} = 1 + \frac{6\pi}{\omega} \text{Im} \left[ \frac{ik_1\mu_1}{8\pi} \sum_{n=0}^{\infty} (2n+1) B_M^{11} \left( z_n^{(1)}(kr) \right)^2 + B_N^{11} \left( \frac{1}{kr} \frac{d}{dr} \left[ r z_n^{(1)}(kr) \right] \right)^2 \right], \quad (41b)$$

where  $\Gamma_0 = \frac{\omega_A^3 d_A^2}{3\hbar\pi\epsilon_0 c^3}$  is the rate of spontaneous emission in free space.

Fig. 2 illustrates the variation of the normalized rate of the radial spontaneous decay given by Eq. (41) for a radially oriented transition dipole moment as a function of the dimensionless parameters  $\omega/\omega_0$  and  $r\omega_0/c$ . According to the experimental data reported in [40] for the spontaneous emission rate of a quantum dot in the microwave



frequency region and with regards that the majority of the cloak devices have been constructed in this frequency range, the material parameters of the constructed cloak in [3] are used here to study the performance of the cloak quantum mechanically.

In Fig. 2, the cyan curve represents the exact result in which the exact Green tensor (A16a) with the coefficients (A18) are inserted in Eq. (41a), whereas, the green and the blue curves correspond to the cases that the cloak is approximately modeled by 16 and 22 spherical thin layers, respectively, and  $\Gamma^\perp/\Gamma_0$  are calculated by making use of the coefficients (A29). The radial component of the material parameters of each layer are given in Table. (I). To examine the performance of the cloak shell, the normalized spontaneous decay  $\Gamma^\perp/\Gamma_0$  is also depicted in the absence of the cloak. The corresponding plot is indicated by the red dashed curve. For comparison, the spontaneous decay rate in free space is shown by black dashed line.

From Fig. 2 (a), we observe a significant enhancement of the decay rate in the vicinity of the cloak resonance frequency. It reveals that the cloak near the resonance frequency not only conceals the object but also makes it more visible. In contrast, far from the cloak resonance frequency, the spontaneous emission of the atom differs from the free space value by about 0.1. While, the variations are in the order of 0.01 in the absence of the cloak. It seems that the performance of the cloak shell is quite well far from the cloak resonance frequency. But, with decreasing distance between the atom and the cloak, near-field effects become important and the spontaneous emission reveals the strong enhancement, as seen in Fig. 2(b). It describes non-radiative decay, i.e., the energy transfer from the atom to the cloak [41], and causes the hidden object to appear. The enhancement decreases by increasing distance between the atom and the cloak and all curves asymptotically tend to the free space value when  $r \rightarrow \infty$ .

From the classically researches reported on the cloak devices, we expect that the combination of the cloak and the object had the properties of free space when viewed externally. Here, if the cloak can hide the object successfully, the spontaneous decay rate should be unchanged as if there were nothing. Whereas, our results demonstrate that there is a strikingly difference with the free space value when the atom located in close distance to the cloak and also near the cloak resonance frequency. So, just far from the cloak resonance frequency and moderate distance, the object plus the cloak are rather invisible.

Comparing the cyan curve with the green and the blue curves in Fig. 2 show clearly that as the layers are made thinner by increasing the number of layers from 14 to 22, the agreement between the approximate results and the exact one increases. Since, the layered cloak with a large number of layers has nearly the same property as the equivalent cloak shell. This means that we are able to use a concentric layered structure to realize a spherical cloak shell. However, by increasing the number of layers, cal-

culating the electromagnetic Green tensor of the system becomes computationally time-consuming due to the numerically demands of determining the coefficients (A29). In following, we therefore restrict our attention only to the exact Green tensor Eq.(A16a) together with the coefficients which are given by Eq. (A18).

The effect of different hidden objects covered by the cloak shell on the spontaneous emission rate is illustrated in Fig. 3. The different objects enter to our calculations by attributing different values to the factor  $\alpha$  of the material parameters. By comparing the green and the cyan curves in Figs. 3 (a) and (b) it is seen that with increasing the constant factor  $\alpha$  from 1.3 to 1.9 in the absence of the cloak, changes in amplitude of the spontaneous decay rate severely enhance. While, in agreement with the classical results, the blue dashed and red dotted curves stay without any changes in the presence of the cloak. Therefore, the cloak acts independent of the object to be cloaked.

For a tangentially oriented dipole moment, the normalized rate of the spontaneous decay given by Eq. (41b) are plotted in Figs. 3 (c) and 3 (d) as a function of the dimensionless parameters  $\omega/\omega_0$  and  $r\omega_0/c$ , respectively. From Fig. 3 (c), it is seen that the spontaneous decay rate, except a subtle decrease in amplitude, shows a similar behavior as in Fig. 3 (a). For instance, at frequency  $\omega/\omega_0 = 0.5$ , the normalized decay rate (41b) for the objects with factors  $\alpha = 1.3$  and  $\alpha = 1.9$  are in the order of 1.04 and 1.07 in the absence of the cloak, respectively, and order of 1.01 in the presence of the cloak. While, these values for a radially oriented dipole moment are in the order of 1.01, 1.16 and 1.04 respectively.

Fig. 3 (d) represents that the results with only slight reduction in amplitude are similar to Fig. 3 (a), provided that the object surrounded by the cloak shell. In the absence of cloak and close distances to the cloak, there is a noticeable difference between Figs. 3 (b) and 3 (d). Finally, the tangential spontaneous decay rate like the vertical spontaneous decay rate tends to the unit value very far away from the cloak.

As a conclusion of this section, we found that such cloak shells independent of the dipole moment orientation of our probe which is here an excited two level atom, operate quite well far from the cloak resonance frequency and moderate distance. Particularly, the ability of the cloak to conceal an object with larger material parameters is better than when the cloak is absent.

#### IV. SPATIAL DISTRIBUTION OF THE EMITTED-LIGHT INTENSITY

Let us finally examine the influence of the the combination of the cloak shell and the hidden object on the emission pattern of light emitted by the excited atom. The intensity of the spontaneously emitted light registered by a photodetector at position  $r$  and time  $t$  is given

by [32, 41]

$$\mathbf{I}(\mathbf{r}, t) \equiv \langle \psi(t) | \hat{\mathbf{E}}^{(-)}(\mathbf{r}, \omega) \cdot \hat{\mathbf{E}}^{(+)}(\mathbf{r}, \omega) | \psi(t) \rangle. \quad (42)$$

By substituting Eqs. (25) and (31) into the above equation and after some algebraic calculations, we get

$$I(\mathbf{r}, t) = \left| \frac{k_A^2 \mathbf{d}_A}{\pi \varepsilon_0} \cdot \int_0^t dt' \times \left[ C_u(t') \int_0^\infty d\omega \text{Im}[\bar{G}(\mathbf{r}, \mathbf{r}_A, \omega)] e^{-i(\omega - \omega_A)(t-t')} \right] \right|^2. \quad (43)$$

Note that Eq. (43) is valid for both weak and strong coupling regimes. In the weak coupling regime, we can apply the Markov approximation and replace  $C_u(t')$  by  $C_u(t)$ . Thus, Eq.(43) simplifies to

$$I_w(\mathbf{r}, t) = |\mathbf{F}_w(\mathbf{r}, \mathbf{r}_A, \omega)|^2 e^{-\Gamma t}, \quad (44)$$

where the spatial distribution function  $\mathbf{F}_w(\mathbf{r}, \mathbf{r}_A, \omega)$  is defined as

$$\mathbf{F}_w(\mathbf{r}, \mathbf{r}_A, \omega) = -\frac{i\omega_A^2 \mathbf{d}_A}{c^2 \varepsilon_0} \left[ \bar{G}(\mathbf{r}, \mathbf{r}_A, \omega) - \frac{P}{\pi} \int_0^\infty d\omega \frac{\text{Im}\bar{G}(\mathbf{r}, \mathbf{r}_A, \omega)}{\omega + \omega_A} \right]. \quad (45)$$

For the strong atom-field coupling, Eq. (43) on the basis of Eq. (39) changes to

$$I_s(\mathbf{r}, t) = |\mathbf{F}_s(\mathbf{r}, \mathbf{r}_A, \omega)|^2 e^{-2\delta\omega_c t} \sin^2\left(\frac{\Omega t}{2}\right), \quad (46)$$

where the spatial distribution function  $\mathbf{F}_s(\mathbf{r}, \mathbf{r}_A, \omega)$  is given by

$$\mathbf{F}_s(\mathbf{r}, \mathbf{r}_A, \omega) = -\frac{i\omega_A^2 \mathbf{d}_A}{\pi c^2 \varepsilon_0} \frac{\delta\omega_c}{\Omega} \text{Im} \left[ \bar{G}(\mathbf{r}, \mathbf{r}_A, \omega_c) \right]. \quad (47)$$

In the above equations, the subscripts  $w$  and  $s$  refer to the case where the excited atom is weakly and strongly coupled to the field, respectively.

Let us restrict our attention to a radially oriented transition dipole moment. In this case, by simply substituting Eq. (40b) into Eq. (45), we arrive at

$$\begin{aligned} \mathbf{F}_w^\perp(\mathbf{r}, \mathbf{r}_A, \omega) &= \frac{k_A^3 \mathbf{d}_A}{4\pi \varepsilon_0} \sum_{n=1}^\infty \frac{(2n+1)}{k_A r_A} \\ &\times \left[ j_n(k_A r_A) + B_N^{11} h_n^{(1)}(k_A r_A) \right] \\ &\times \left[ \mathbf{e}_r \frac{n(n+1)h_n^{(1)}(k_A r)}{k_A r} P_n(\cos\theta) \right. \\ &\left. - \mathbf{e}_\theta \frac{[k_A r h_n^{(1)}(k_A r)]'}{(k_A r)} \sin\theta P_n'(\cos\theta) \right], \quad (48a) \end{aligned}$$

$$\mathbf{F}_s^\perp(\mathbf{r}, \mathbf{r}_A, \omega) = \delta\omega_c / \Omega \text{Im}[\mathbf{F}_w^\perp(\mathbf{r}, \mathbf{r}_A, \omega)]. \quad (48b)$$

The far-field contribution of the emission pattern  $|\mathbf{F}^\perp(\mathbf{r}, \mathbf{r}_A, \omega)|^2 / (k_A^3 \mathbf{d}_A / 4\pi \varepsilon_0)^2$  for a radially oriented transition dipole moment in weak and strong coupling regimes is plotted in Fig. 4 for two cases: at the cloak resonance  $\omega = \omega_0$  and far from the cloak resonance  $\omega = 0.01\omega_0$ . The cyan and the green curves represent the influence of the central hidden object with different material parameters  $\alpha = 1.3$  and  $\alpha = 1.9$  on the intensity of the spontaneously emitted light, while the results for the combination of the cloak and object are depicted by the blue dashed and red dash-dotted curves. For more clarification, our results are compared with the yellow curve associated with the spontaneous emission pattern of the excited atom in free space.

In Fig. 4, the emission patterns exhibit a symmetry with respect to the plane  $\theta = 0$  because of our symmetry system. In part (a) of this figure, far from the cloak resonance frequency and in the weak coupling regime, they give rise to an approximately one-lobe structure which the most pronounced amounts of the intensity placed in the interval  $0 < \theta < 45^\circ$ . We observe that the emission patterns in presence of the cloaking shell and independent of the object coincide with the corresponding plot in free space, while in absence of the cloak the emission patterns associated to the object with material parameter  $\alpha = 1.3$  and  $\alpha = 1.9$  are not only mismatch with each other but also with the plot in free space.

Within the cloak resonance frequency, a strikingly different behavior is observed and the pattern of emission changes to a two-lobe structure, as it is seen in Fig. 4(b). Obviously, a photon that is spontaneously emitted is almost certainly absorbed in resonant interaction and does not contribute to the far field. Consequently, the emission intensity decreases. However, the absorption is substantial in presence of the combination of the cloak and the object such that the emission intensity independent of the objects reduces about in the order of 2, because of the emitted light is in resonance with both the cloak shell and the object. Furthermore, we observe that the emission patterns bent away from the cloak shell as compared to that case in free space. Although, this inclination behavior is lesser when the cloak is absent.

In Fig. 4(c), the emission patterns in the strong coupling regime and far from the resonance frequency resembles that observed for nonresonant interaction in the weak coupling regime (Fig. 4(a)), but the emission intensity is reduced by magnitude order of  $10^3$ , since, the absorption losses have a more prominent role in strong coupling regime. It is seen that the cyan and green curves in strong coupling regime, which is associated to different hidden object  $\alpha = 1.3$  and  $\alpha = 1.9$ , coincide with each other such that a slight difference remains between plots with and without the cloak near  $\theta = 0$ . Therefore, the similarity between the plots far from the cloak resonance frequency is fairly good even in the strong regime and the previous results obtained by studying the spontaneous emission rate are achieved.

The interpretation of the curves in Fig. 4(d) is quite

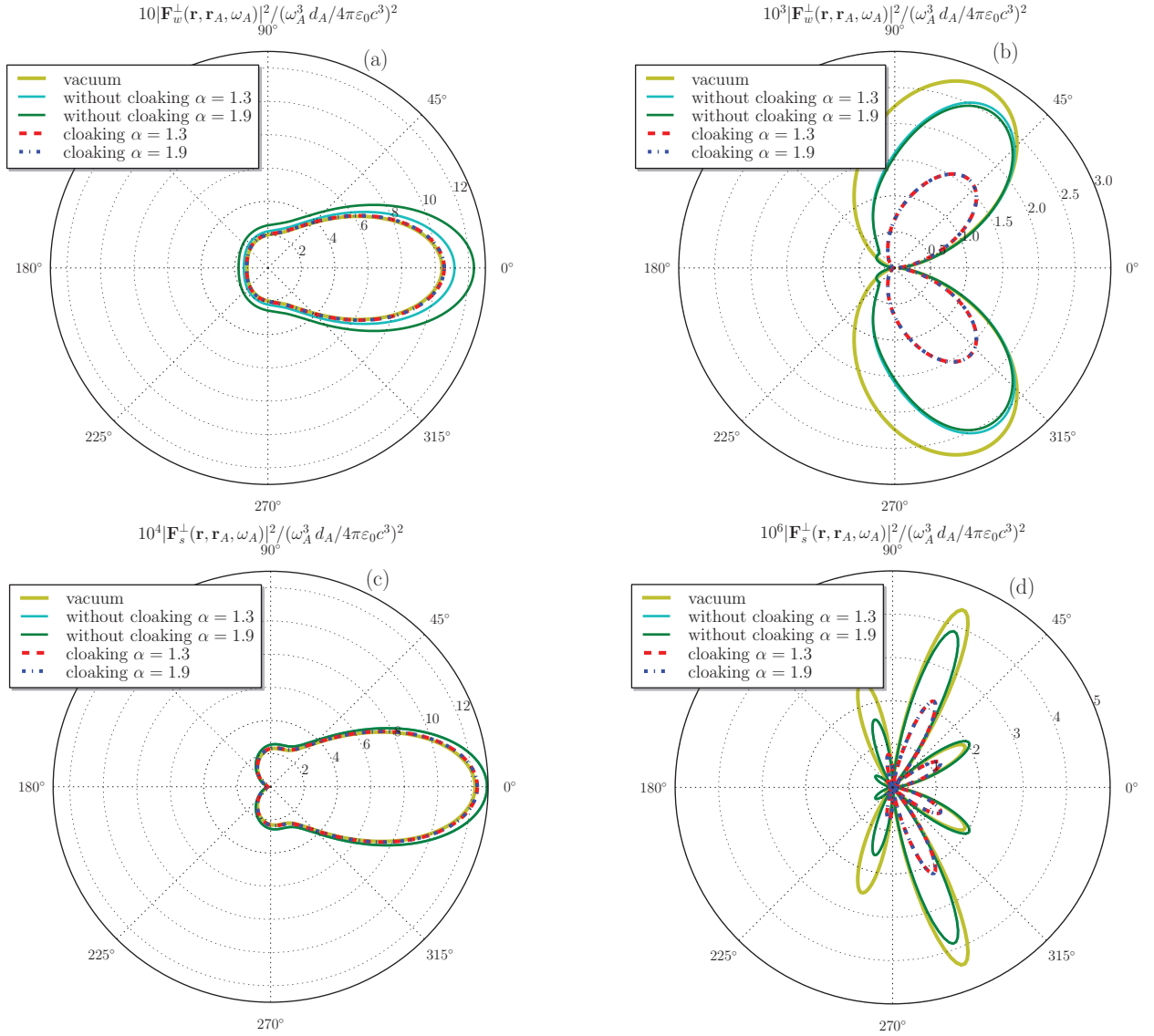


FIG. 4. Polar diagram of the normalized far-field emission pattern  $|\mathbf{F}_w(\mathbf{r}, \mathbf{r}_A, \omega)|^2 / (k_A^3 d_A / 4\pi\epsilon_0 c^3)^2$  for a radially oriented transition dipole moment that is placed at  $r_A = 4.7c/\omega_0$  and the emission intensity is measured at the location  $r = 20c/\omega_0$  apart from the cloak. The left and right panels correspond to nonresonant ( $\omega = 0.01\omega_0$ ) and resonant ( $\omega = \omega_0$ ) interaction of the excited atom with the field, respectively. Upper panels are for weak coupling regime and lower panels for the strong coupling regime. The size of the cloak and the material parameters of the cloaking device are identical to those used in Fig. 2. We have chosen  $\delta\omega_c = 0.01\omega_0$ .

similar to that of the plots in Fig. 4(b). Of course, some differences are also observed: Two-lobe structure changes into a several lobe structure and unlike to that observed in free space some unwanted radiation is appeared near  $\theta = \pi$  when the cloak shell is absent. It seems that the performance of the combination of the cloak and the object is fairly good in this direction. Thus, the effect of the cloaking device in the resonance cloak frequency and strong coupling regime reveals that the object becomes more visible.

## V. CONCLUSION

We have developed a formalism for studying the quantum features of an invisibility metamaterials cloak. We have given a systematic analysis of spontaneous decay of an excited two-level atom placed in the vicinity of the spherical cloak. For this purpose, we have extended the canonical quantization scheme which was presented in [24]- [27], to the case that the electromagnetic field interact with charge particles in the presence of the dispersive, absorptive, anisotropic and inhomogeneous magnetodielectric medium.

Then we have used this rigorous formalism to investigate the spontaneous decay of the excited atom near a spherical cloak surrounded the hidden objects in two regimes: weak coupling in which the excited atomic state decays exponentially, and the strong coupling regime which is realized when the atomic transition frequency is close to the cloak resonance frequency. Since, the spontaneous emission is stated in terms of the electromagnetic Green tensor, we have extracted the Green tensor via two methods: exact and discrete methods. The former is directly computed for our system, while the latter one calculated by modeling the cloak shell through concentric layered structure of thin and extending the relations in [35]- [37].

In study of the spontaneous decay rate of the excited atom near the cloaking device, we have assumed that the material absorbtion and dispersion of the cloak and also the central object is modeled by Lorentz model. It is seen that the spontaneous decay rate is in agreement with that case in free space at moderate distance and far from the cloak resonance frequency and thus the cloak shell works well to conceal the object. Moreover, we observed that the performance of the cloak is independent of the central object.

Further investigations are also necessary in order to give a detailed analysis of metamaterial invisibility cloak in the quantum mechanic domain. So, we have discussed the spatial distribution of the spontaneously emitted light in the weak and strong coupling regime. Far from the cloak resonance frequency and within both weak and strong coupling regimes, it is seen that the emission patterns in the presence of the cloak coincide with the corresponding plot in free space. Therefore, the performance of the cloak shell to render the object invisible is good even in strong regime. At near the resonance frequency, the cloak is highly dissipative and dispersive so that the emission pattern takes a form that is almost different from the vacuum pattern which causes the hidden object became more visible than the results observed in the classical domain.

## ACKNOWLEDGMENT

M. Morshed Behbahani, E. Amooghorban and A. Mahdifar wish to thank the Shahrekord University for their support.

## Appendix A: Green tensor of spherical invisibility cloaking

In this appendix, we extract the electromagnetic Green tensor for an inhomogeneous, anisotropic and dispersive spherical cloak shell which enclosed a homogeneous and isotropic medium as a central object should be hidden.

Considering Eqs. (12) and the constitutive relations followed after it, the Maxwell equations for a source-free medium are given by

$$\nabla \times [(\varepsilon_0 \bar{\varepsilon})^{-1} \cdot \mathbf{D}] = -i\omega \mathbf{B}, \quad (\text{A1a})$$

$$\nabla \times [(\mu_0 \bar{\mu})^{-1} \cdot \mathbf{B}] = i\omega \mathbf{D}. \quad (\text{A1b})$$

We decompose the fields into TE and TM modes with respect to  $\hat{r}$  by introducing the scalar potentials as

$$\mathbf{B}_{TM} = \nabla \times (\hat{r} \psi_{TM}), \quad (\text{A2a})$$

$$\mathbf{D}_{TE} = -\nabla \times (\hat{r} \psi_{TE}), \quad (\text{A2b})$$

$$\mathbf{B}_{TE} = \frac{1}{i\omega} \left\{ \nabla \times [(\varepsilon_0 \bar{\varepsilon})^{-1} \cdot \nabla \times (\hat{r} \psi_{TE})] \right\}, \quad (\text{A2c})$$

$$\mathbf{D}_{TM} = \frac{1}{i\omega} \left\{ \nabla \times [(\mu_0 \bar{\mu})^{-1} \cdot \nabla \times (\hat{r} \psi_{TM})] \right\}. \quad (\text{A2d})$$

By inserting Eqs. (A2b) and (A2c) into the Maxwell equation (A1b) and equating the radial components, we can get the wave equation for the scalar potential  $\psi_{TE}$  as follows:

$$\frac{\mu_r}{\mu_t} \frac{\partial^2 \psi_{TE}}{\partial r^2} + \nabla_t^2 \psi_{TE} + \omega^2 \mu_0 \varepsilon_0 \mu_t \varepsilon_r \psi_{TE} = 0. \quad (\text{A3})$$

where

$$\nabla_t^2 = \frac{1}{r^2 \sin \theta} \frac{\partial}{\partial \theta} \left( \sin \theta \frac{\partial}{\partial \theta} \right) + \frac{1}{r^2 \sin^2 \theta} \frac{\partial^2}{\partial \phi^2}. \quad (\text{A4})$$

In a similar way, the wave equation for the scalar potential  $\psi_{TM}$  is obtained by substituting Eqs. (A2a) and (A2d) into Eq. (A1a) as

$$\frac{\varepsilon_r}{\varepsilon_t} \frac{\partial^2 \psi_{TM}}{\partial r^2} + \nabla_t^2 \psi_{TM} + \omega^2 \mu_0 \varepsilon_0 \mu_t \varepsilon_r \psi_{TM} = 0. \quad (\text{A5})$$

An interesting thing arises when the cloak parameters (29) are inserted into above equations. In this case, we have:  $\frac{\mu_t}{\mu_r} = \frac{\varepsilon_t}{\varepsilon_r} = \left(\frac{r}{r-b}\right)^2$ . Therefore, the wave equations (A3) and (A5) for both scalar potentials  $\psi_{TE}$  and  $\psi_{TM}$  become identical. Hereafter, we drop the subscript TE and TM, and specify the scalar potential by  $\psi$ . To solve the scalar wave equation, we use the separation of variable method and assuming  $\psi = f(r)g(\theta)h(\phi)$ . We find that  $g(\theta)$  and  $h(\phi)$  are, respectively, associated Legendre polynomials and harmonic functions, and  $f(r)$  is the solution of the following equation:

$$\left\{ \frac{\partial^2}{\partial r^2} + \left[ k_t^2 - \beta \frac{n(n+1)}{r^2} \right] \right\} f(r) = 0, \quad (\text{A6})$$

where  $k_t = \frac{\omega}{c} \sqrt{\varepsilon_t \mu_t}$  and  $\beta = \frac{\mu_t}{\mu_r} = \frac{\varepsilon_t}{\varepsilon_r}$  is anisotropic ratio of the cloak. We will solve the above equation in two ways: *exact* method and *discrete* method. In the following, we briefly illustrate these methods.

### 1. Exact method

By using the relation between material parameters specified in (29), i.e.  $\beta = \left(\frac{r}{r-b}\right)^2$ , Eq. (A6) in the cloak

shell is converted to the Riccati-Bessel equation

$$\left\{ \frac{\partial^2}{\partial r^2} + \left[ k_t^2 - \frac{n(n+1)}{(r-b)^2} \right] \right\} f(r) = 0. \quad (\text{A7})$$

The solution of the above equation is of the form

$$f(r) = k_t(r-b)z_n^{(l)}(k_t(r-b)), \quad (\text{A8})$$

where the superscripts  $l = 0$  and  $l = 1$  refer to the Riccati-Bessel functions of the first and the third kind, respectively. In other word, the superscripts (0) and (1) denote that the first-type spherical Bessel function,  $j_n$ , and the third-type spherical Bessel function or the first-type spherical Hankel function,  $h_n^{(1)}$ , should be chosen in Eq. (A8). From the above analysis, we find the general solution of Eq. (A3) in the cloak shell

$$\begin{aligned} \psi^{cl} = & \sum_{m,n} a_{m,n} k_t(r-b) j_n(k_t(r-b)) \\ & \times P_n^m(\cos \theta) \begin{pmatrix} \cos \\ \sin \end{pmatrix} m\phi. \end{aligned} \quad (\text{A9})$$

Let us consider TE/TM decomposition (A2) and the scalar potential (A9), the electromagnetic fields in the cloak shell can therefore be rewritten as

$$\begin{aligned} \mathbf{E}^{cl} = & \mathbf{E}_{TE}^{cl} + \mathbf{E}_{TM}^{cl} \\ = & \sum_{m,n} D_{m,n} a_{m,n} \left[ \frac{k_t}{\varepsilon_0 \varepsilon_t} M_{\varepsilon mn}^{(cl)}(k_t) + \frac{\omega}{i} N_{\varepsilon mn}^{(cl)}(k_t) \right], \end{aligned} \quad (\text{A10a})$$

$$\begin{aligned} \mathbf{H}^{cl} = & \mathbf{H}_{TE}^{cl} + \mathbf{H}_{TM}^{cl} \\ = & -i \sqrt{\frac{\varepsilon_t}{\mu_t}} \sum_{m,n} D_{m,n} a_{m,n} \left[ M_{\varepsilon mn}^{(cl)}(k_t) + N_{\varepsilon mn}^{(cl)}(k_t) \right]. \end{aligned} \quad (\text{A10b})$$

where  $D_{m,n} = (2 - \delta_m^0) \frac{2n+1}{n(n+1)} \frac{(n-m)!}{(n+m)!}$ ,  $M_{\varepsilon mn}^{(cl)}$  and  $N_{\varepsilon mn}^{(cl)}$  are the modified spherical vector wave functions corresponding to the cloak region,  $b < r < a$ , and defined as

$$\begin{aligned} M_{\varepsilon mn}^{(cl)}(k_t) = & \frac{r-b}{r} \left[ \mp \frac{m}{\sin \theta} z_n^{(l)}(k_t(r-b)) \right. \\ & \times P_n^m(\cos \theta) \begin{pmatrix} \sin m\phi \\ \cos m\phi \end{pmatrix} \hat{\theta} \\ & \left. - \frac{dP_n^m(\cos \theta)}{d\theta} z_n^{(l)}(k_t(r-b)) \begin{pmatrix} \cos m\phi \\ \sin m\phi \end{pmatrix} \hat{\phi} \right], \end{aligned} \quad (\text{A11a})$$

$$\begin{aligned} N_{\varepsilon mn}^{(cl)}(k_t) = & \left[ \frac{n(n+1)}{k_t(r-b)} z_n^{(l)}(k_t(r-b)) \right. \\ & \times P_n^m(\cos \theta) \begin{pmatrix} \cos m\phi \\ \sin m\phi \end{pmatrix} \hat{r} \\ & + \frac{1}{kr} \frac{d[(r-b)z_n^{(l)}(k_t(r-b))]}{dr} \\ & \times \left[ \frac{dP_n^m(\cos \theta)}{d\theta} \begin{pmatrix} \cos m\phi \\ \sin m\phi \end{pmatrix} \hat{\theta} \right. \\ & \left. \mp \frac{m}{\sin \theta} P_n^m(\cos \theta) \begin{pmatrix} \sin m\phi \\ \cos m\phi \end{pmatrix} \hat{\phi} \right]. \end{aligned} \quad (\text{A11b})$$

Now with the solution (A9) for the cloak shell, we can also get the field expressions in the regions  $r > a$  and  $r < b$  [see Fig. 1(a)]. Because these two regions are, respectively, free space and the isotropic and homogeneous magnetodielectric medium, the medium parameters consequently does not vary with radius. So, similar to consideration in [37], the corresponding spherical vector wave functions can be obtained by simple replacement

$$\begin{aligned} N_{\varepsilon mn}^{(cl)}(k_t), M_{\varepsilon mn}^{(cl)}(k_t) \longrightarrow & N_{\varepsilon mn}(k_{1,3}), M_{\varepsilon mn}(k_{1,3}), \\ k_t(r-b) \longrightarrow & k_{1,3}r. \end{aligned} \quad (\text{A12})$$

Here the index 1 and 3 refer to the regions  $r > a$  and  $r < b$ , respectively. Moreover, we have  $k_1 = \frac{\omega}{c}$  and  $k_3 = \frac{\omega}{c} \sqrt{\varepsilon_3 \mu_3}$ . With these in mind, the spherical vector wave functions for this two regions are written as

$$\begin{aligned} M_{\varepsilon mn}(k_{1,3}) = & \left[ \mp \frac{m}{\sin \theta} z_n^{(l)}(k_{1,3}r) P_n^m(\cos \theta) \begin{pmatrix} \sin m\phi \\ \cos m\phi \end{pmatrix} \hat{\theta} \right. \\ & \left. - \frac{dP_n^m(\cos \theta)}{d\theta} z_n^{(l)}(k_{1,3}r) \begin{pmatrix} \cos m\phi \\ \sin m\phi \end{pmatrix} \hat{\phi} \right], \end{aligned} \quad (\text{A13a})$$

$$\begin{aligned} N_{\varepsilon mn}(k_{1,3}) = & \frac{n(n+1)}{k_{1,3}r} z_n^{(l)}(k_{1,3}r) P_n^m(\cos \theta) \begin{pmatrix} \cos m\phi \\ \sin m\phi \end{pmatrix} \hat{r} \\ & + \frac{1}{kr} \frac{d[rz_n^{(l)}(k_{1,3}r)]}{dr} \\ & \times \left[ \frac{dP_n^m(\cos \theta)}{d\theta} \begin{pmatrix} \cos m\phi \\ \sin m\phi \end{pmatrix} \hat{\theta} \right. \\ & \left. \mp \frac{m}{\sin \theta} P_n^m(\cos \theta) \begin{pmatrix} \sin m\phi \\ \cos m\phi \end{pmatrix} \hat{\phi} \right]. \end{aligned} \quad (\text{A13b})$$

In terms of the spherical vector wave functions specified in (A11) and (A13), the Green tensor of system can be

constructed. Making use of the method of scattering superposition [35], the Green tensor may be separated into two parts as

$$\bar{\bar{G}}(\mathbf{r}, \mathbf{r}', \omega) = \bar{\bar{G}}_V(\mathbf{r}, \mathbf{r}', \omega) + \bar{\bar{G}}_S(\mathbf{r}, \mathbf{r}', \omega), \quad (\text{A14})$$

where  $\bar{\bar{G}}_V(\mathbf{r}, \mathbf{r}', \omega)$  and  $\bar{\bar{G}}_S(\mathbf{r}, \mathbf{r}', \omega)$  represent the unbounded and the scattering Green tensor, respectively. The former describes the contribution due to the source in the infinite homogeneous space while the latter corresponds the contribution of the source due to the presence of the cloak interfaces. In this paper, the radiation source is located in the free space (region 1), therefore, we only require the unbounded Green tensor in the vacuum i.e.,  $\bar{\bar{G}}_0(\mathbf{r}, \mathbf{r}', \omega)$ . Following the procedure given by Tai [35] for the magnetic and the electric type of dyadic Green function, the unbounded Green tensor under the spher-

ical coordinate system can be expressed for  $r \leq r'$  as follows:

$$\begin{aligned} \bar{\bar{G}}_0(\mathbf{r}, \mathbf{r}', \omega) &= \frac{-\hat{r}\hat{r}}{\omega^2 \varepsilon_0 \varepsilon_r} \delta(r - r') + \frac{ik_1 \mu_0 \mu_1}{4\pi} \sum_{n=0}^{\infty} \sum_{m=0}^{\infty} D_{m,n} \\ &\times \begin{cases} M_{\varepsilon mn}^{(1)}(k_1) M_{\varepsilon mn}'^{(1)}(k_1) + N_{\varepsilon mn}^{(1)}(k_1) N_{\varepsilon mn}'^{(1)}(k_1), & r \geq r', \\ M_{\varepsilon mn}(k_1) M_{\varepsilon mn}'^{(1)}(k_1) + N_{\varepsilon mn}(k_1) N_{\varepsilon mn}'^{(1)}(k_1), & r \leq r', \end{cases} \end{aligned} \quad (\text{A15})$$

where the prime denotes the coordinates  $(r', \theta', \varphi')$  of the source. With regards to the fact that the radiation source is embedded inside the free space and taking into account the multiple transmission and reflection effects, we can construct the scattering Green tensor for  $f = 1, 2, 3$  as follows:

$$\bar{\bar{G}}_s^{(11)}(\mathbf{r}, \mathbf{r}', \omega) = \frac{ik_1 \mu_0 \mu_1}{4\pi} \sum_{n=0}^{\infty} \sum_{m=0}^n D_{m,n} \left\{ \left[ M_{\varepsilon mn}^{(1)}(k_1) B_M^{11} M_{\varepsilon mn}'^{(1)}(k_1) \right] + \left[ N_{\varepsilon mn}^{(1)}(k_1) B_N^{11} N_{\varepsilon mn}'^{(1)}(k_1) \right] \right\}, \quad (\text{A16a})$$

$$\begin{aligned} \bar{\bar{G}}_s^{(21)}(\mathbf{r}, \mathbf{r}', \omega) &= \frac{ik_1 \mu_0 \mu_1}{4\pi} \sum_{n=0}^{\infty} \sum_{m=0}^n D_{m,n} \left\{ \left[ M_{\varepsilon mn}^{(cl)}(k_t) B_M^{21} M_{\varepsilon mn}'^{(1)}(k_1) \right] + \left[ N_{\varepsilon mn}^{(cl)}(k_t) B_N^{21} N_{\varepsilon mn}'^{(1)}(k_1) \right] \right\} \\ &+ \left[ M_{\varepsilon mn}^{(cl)}(k_t) D_M^{21} M_{\varepsilon mn}'^{(1)}(k_1) \right] + \left[ N_{\varepsilon mn}^{(cl)}(k_t) D_N^{21} N_{\varepsilon mn}'^{(1)}(k_1) \right], \end{aligned} \quad (\text{A16b})$$

$$\bar{\bar{G}}_s^{(31)}(\mathbf{r}, \mathbf{r}', \omega) = \frac{ik_1 \mu_0 \mu_1}{4\pi} \sum_{n=0}^{\infty} \sum_{m=0}^n D_{m,n} \left\{ \left[ M_{\varepsilon mn}(k_3) D_M^{31} M_{\varepsilon mn}'^{(1)}(k_1) \right] + \left[ N_{\varepsilon mn}(k_3) D_N^{31} N_{\varepsilon mn}'^{(1)}(k_1) \right] \right\}, \quad (\text{A16c})$$

where the  $B_{M,N}$  and  $D_{M,N}$  are the coefficients of the scattered Green tensor to be determined. To determine the unknown coefficients in (A16), the boundary conditions satisfied by the Green tensor in the spherical interfaces should be used. These boundary conditions at the spherical interfaces  $r = a$  and  $r = b$  are given as following to ensure continuity of tangential electric and magnetic fields:

$$\hat{r} \times \left[ \bar{\bar{G}}_0 + \bar{\bar{G}}_s^{(11)} \right] \Big|_{r=b} = \hat{r} \times \bar{\bar{G}}_s^{(21)} \Big|_{r=b}, \quad (\text{A17a})$$

$$\hat{r} \times \bar{\bar{G}}_s^{(21)} \Big|_{r=a} = \hat{r} \times \bar{\bar{G}}_s^{(31)} \Big|_{r=a}, \quad (\text{A17b})$$

$$\frac{1}{\mu_1} \hat{r} \times \nabla \times \left[ \bar{\bar{G}}_0 + \bar{\bar{G}}_s^{(11)} \right] \Big|_{r=b} = \hat{r} \times \left[ \bar{\mu}_2^{-1} \cdot \nabla \times \bar{\bar{G}}_s^{(21)} \right] \Big|_{r=b}, \quad (\text{A17c})$$

$$\hat{r} \times \left[ \bar{\mu}_2^{-1} \cdot \nabla \times \bar{\bar{G}}_s^{(21)} \right] \Big|_{r=a} = \frac{1}{\mu_3} \hat{r} \times \nabla \times \bar{\bar{G}}_s^{(31)} \Big|_{r=a}. \quad (\text{A17d})$$

In this paper only the scattering coefficients  $B_{M,N}^{11}$  are of interest and must be determined. Since the decay rate of the excited atom, which is located in free space in our case, depends on the Green tensor of system at the position of the atom, therefore, the source and the field points are located in region 1. By inserting Eq. (A16) into Eq. (A17) and solving the obtained equations, the

unknown coefficients  $B_{M,N}^{11}$  are derived as

$$B_{M,N}^{11} = - \frac{T_{P1}^{H,V} R_{F1}^{H,V} + T_{F1}^{H,V} R_{F2}^{H,V}}{R_{F2}^{H,V} R_{P1}^{H,V} T_{F1}^{H,V} + T_{P1}^{H,V}}, \quad (\text{A18})$$

where the superscript  $F$  and  $P$  stand for the centrifugal and centripetal waves and the TE and TM waves represented by the subscripts  $H$  and  $V$ , respectively. The

reflection and transition coefficients  $R_{F,P}^{H,V}$  and  $T_{F,P}^{H,V}$  in-

troduced in Eq. (A18) are defined as

$$\begin{aligned}
T_{F1}^H &= \frac{\eta_1 \mu_1 k_2 (\partial \mathfrak{S}_2 \hbar_2 - \mathfrak{S}_2 \partial \hbar_2)}{\mu_1 k_2 \partial \mathfrak{S}_2 \hbar_1 - \mu_2 k_1 \mathfrak{S}_2 \partial \hbar_1}, & T_{F1}^V &= \frac{\eta_1 \mu_1 k_2 (\mathfrak{S}_2 \partial \hbar_2 - \partial \mathfrak{S}_2 \hbar_2)}{\mu_1 k_2 \mathfrak{S}_2 \partial \hbar_1 - \mu_2 k_1 \partial \mathfrak{S}_2 \hbar_1}, \\
T_{P1}^V &= \frac{\eta_1 \mu_1 k_2 (\partial \mathfrak{S}_2 \hbar_2 - \mathfrak{S}_2 \partial \hbar_2)}{\mu_1 k_2 \partial \mathfrak{S}_1 \hbar_2 - \mu_2 k_1 \mathfrak{S}_1 \partial \hbar_2}, & T_{P1}^H &= \frac{\eta_1 \mu_1 k_2 (\partial \mathfrak{S}_2 \hbar_2 - \partial \mathfrak{S}_2 \hbar_2)}{\mu_1 k_2 \mathfrak{S}_1 \partial \hbar_2 - \mu_2 k_1 \partial \mathfrak{S}_1 \hbar_2}, \\
R_{F2}^H &= \frac{\mu_2 k_3 \partial \mathfrak{S}_3 \mathfrak{S}_2 - \mu_3 k_2 \partial \mathfrak{S}_2 \mathfrak{S}_3}{\mu_2 k_3 \partial \mathfrak{S}_3 \hbar_2 - \mu_3 k_2 \mathfrak{S}_3 \partial \hbar_2}, & R_{F2}^V &= \frac{\mu_2 k_3 \mathfrak{S}_3 \partial \mathfrak{S}_2 - \mu_3 k_2 \mathfrak{S}_2 \partial \mathfrak{S}_3}{\mu_2 k_3 \mathfrak{S}_3 \partial \hbar_2 - \mu_3 k_2 \partial \mathfrak{S}_3 \hbar_2}, \\
R_{F1}^V &= \frac{\mu_1 k_2 \mathfrak{S}_2 \partial \mathfrak{S}_1 - \mu_2 k_1 \mathfrak{S}_1 \partial \mathfrak{S}_2}{\mu_1 k_2 \mathfrak{S}_2 \partial \hbar_1 - \mu_2 k_1 \partial \mathfrak{S}_2 \hbar_1}, & R_{F1}^H &= \frac{\mu_1 k_2 \partial \mathfrak{S}_2 \mathfrak{S}_1 - \mu_2 k_1 \partial \mathfrak{S}_2 \mathfrak{S}_1}{\mu_1 k_2 \partial \mathfrak{S}_2 \hbar_1 - \mu_2 k_1 \mathfrak{S}_2 \partial \hbar_1}, \\
R_{P1}^H &= \frac{\mu_1 k_2 \partial \hbar_2 \hbar_1 - \mu_2 k_1 \hbar_2 \partial \hbar_1}{\mu_1 k_2 \partial \hbar_2 \mathfrak{S}_1 - \mu_2 k_1 \hbar_2 \partial \mathfrak{S}_1}, & R_{P1}^V &= \frac{\mu_1 k_2 \partial \hbar_1 \hbar_2 - \mu_2 k_1 \hbar_1 \partial \hbar_2}{\mu_1 k_2 \hbar_2 \partial \mathfrak{S}_1 - \mu_2 k_1 \partial \hbar_2 \mathfrak{S}_1}.
\end{aligned} \tag{A19}$$

In Eq. (A19), the following parameters have been used to simplify the symbolic calculations

$$\begin{aligned}
\mathfrak{S}_1 &= j_n(k_1 r), & \mathfrak{S}_t &= j_n(k_t(r-b)), \\
\hbar_1 &= h_n^{(1)}(k_t r), & \hbar_t &= h_n^{(1)}(k_t(r-b)), \\
\partial \mathfrak{S}_1 &= \frac{1}{\rho} \frac{d[\rho j_n(\rho)]}{d\rho} \Big|_{\rho=k_1 r}, & \partial \mathfrak{S}_t &= \frac{1}{\rho} \frac{d[\rho j_n(\rho)]}{d\rho} \Big|_{\rho=k_t(r-b)}, \\
\partial \hbar_1 &= \frac{1}{\rho} \frac{d[\rho h_n^{(1)}(\rho)]}{d\rho} \Big|_{\rho=k_1 r}, & \partial \hbar_t &= \frac{1}{\rho} \frac{d[\rho h_n^{(1)}(\rho)]}{d\rho} \Big|_{\rho=k_t(r-b)}.
\end{aligned} \tag{A20}$$

## 2. Discrete method

As shown in Fig. 1(b), we model the cloak shell by a large number of the spherical thin layers with constant material parameters whose radial component in each layer increases outward according to Eq. (29). In this case, which is an approximation of the exact cloak, we can choose the material parameters as

$$\varepsilon_t(\omega) = \mu_t(\omega) = \frac{a}{a-b} \kappa_L(\omega), \tag{A21}$$

$$\varepsilon_r(\omega, f) = \mu_r(\omega, f) = \frac{a}{a-b} \left( \frac{r_{f-1} - b}{r_{f-1}} \right)^2 \kappa_L(\omega). \tag{A22}$$

where  $r_f$  corresponds to the location of the  $f$ th layer. In Table. (I), the radial component of the anisotropic permittivity and permeability (29b) is shown for two cases which is used in Fig. 2 with  $N = 14$  and  $N = 22$  layered cloak. Now, we insert the material parameters (A21) in Eq. (A6) and equating the expression  $n(n+1) \frac{\varepsilon_t}{\mu_t}$  by  $\nu(\nu+1)$ . We find that the solution of the Eqs. (A6) has a similar form according to Eq. (A23), but with a difference that the spherical Bessel function of the  $n$ th order and as well as the radius function  $(r-b)$  replaced by  $\nu = \left[ n(n+1) \frac{\varepsilon_t}{\varepsilon_r} + \frac{1}{4} \right]^{1/2} - \frac{1}{2}$  and  $r$ , respectively. This allow us to write the general solution of Eq. (A3) inside the layered cloak as

$$\psi^{cl} = \sum_{m,n} b_{m,n} k_t r z_\nu(k_t r) P_n^m(\cos \theta) \begin{pmatrix} \cos \\ \sin \end{pmatrix} m\phi. \tag{A23}$$

The analysis similar to that of the electric and magnetic field in Eqs. (A10) shows that the spherical vector wave functions  $M_{\sigma m \nu}^{(cl)}(k_t)$  and  $N_{\sigma m \nu}^{(cl)}(k_t)$  inside the layered cloak can be specified by Eqs. (A13) with the function  $z_n(k_t r)$  replaced by  $z_\nu(k_t r)$ . Of course, these functions remain without any changes outside the cloak. Given that the source is located out of the cloak, i.e.,  $s = 1$ , the scattering Green tensor for the  $f$ th layer is expressed as [36]

$$\begin{aligned}
\bar{G}_s^{(f1)}(\mathbf{r}, \mathbf{r}', \omega) &= \frac{ik_{t,s} \mu \mu_{t,f}}{4\pi} \sum_{n=0}^{\infty} \sum_{m=0}^{\infty} D_{m,n} \\
&\times \left( (1 - \delta_f^N) M_{m\nu}^{(1)}(k_f) \left[ (1 - \delta_f^N) B_M^{f1} M_{m\nu}'^{(1)}(k_1) \right] \right. \\
&+ (1 - \delta_f^N) N_{m\nu}^{(1)}(k_f) \left[ B_N^{f1} N_{m\nu}'^{(1)}(k_1) \right] \\
&+ (1 - \delta_f^1) M_{m\nu}^{(1)}(k_f) \left[ D_M^{f1} M_{m\nu}'^{(1)}(k_1) \right] \\
&\left. + (1 - \delta_f^1) N_{m\nu}^{(1)}(k_f) \left[ D_N^{f1} N_{m\nu}'^{(1)}(k_1) \right] \right). \tag{A24}
\end{aligned}$$

where the superscripts  $f$  denotes the field point located in  $f$ th region. Now, all that remains to be done is to determine the unknown coefficients  $B_{M,N}^{f1}$  and  $D_{M,N}^{f1}$ . As explained in the direct method, the field point in our model is located in region 1. Therefore, we only require the unknown coefficient  $B_{M,N}^{11}$ . The procedure for deriving the coefficients  $B_{M,N}^{11}$  is similar to that obtained in Eq. A18. The boundary conditions should be satisfied by the scattering Green tensor at interfaces  $r = r_f$  and

TABLE I. Radial components of permittivity and permeability of each layer for 22 and 14 multilayered cloak. The material absorption and dispersion of each layer is described by the Lorentz model with parameters that are identical to those used in Fig. 2.

	$(\mu_r = \varepsilon_r)/\kappa_L$	
$f$	$N = 14$	$N = 22$
1	1.000	1.000
2	0.330	0.330
3	0.300	0.310
4	0.260	0.290
5	0.220	0.270
6	0.190	0.240
7	0.150	0.220
8	0.120	0.200
9	0.090	0.180
10	0.060	0.160
11	0.040	0.140
12	0.180	0.120
13	0.005	0.100
14	1.300	0.080
15	—	0.070
16	—	0.050
17	—	0.040
18	—	0.020
19	—	0.015
20	—	0.007
21	—	0.001
22	—	1.300

$r = r_{f+1}$ . Thus, we have

$$\hat{r} \times [\bar{G}_0 + \bar{G}_s^{(fs)}] = \hat{r} \times \bar{G}_s^{(f+1)s} \quad (\text{A25a})$$

$$\hat{r} \times \bar{G}_s^{(fs)} = \hat{r} \times \bar{G}_s^{(f+1)s} \quad (\text{A25b})$$

$$\mu_f^{-1} \hat{r} \times \nabla \times [\bar{G}_0 + \bar{G}_s^{(fs)}] = \hat{r} \times [\bar{\mu}_{f+1}^{-1} \cdot \nabla \times \bar{G}_s^{(f+1)s}] \quad (\text{A25c})$$

$$\hat{r} \times [\bar{\mu}_f^{-1} \cdot \nabla \times \bar{G}_s^{(fs)}] = \mu_{f+1}^{-1} \hat{r} \times \nabla \times \bar{G}_s^{(f+1)s} \quad (\text{A25d})$$

Let us introduce the following transmission matrix

$$[T_{l,f}] = \begin{bmatrix} \frac{1}{T_{E,f}^{H,V}} & \frac{R_{E,f}^{H,V}}{T_{E,f}^{H,V}} \\ \frac{R_{E,f}^{H,V}}{T_{E,f}^{H,V}} & \frac{1}{T_{E,f}^{H,V}} \end{bmatrix}, \quad (\text{A26})$$

where  $l = M, N$  and the reflection and transmission coefficients  $R_{(F,P)f}^{H,V}$  and  $T_{(F,P)f}^{H,V}$  are given by

$$\begin{aligned} T_{Ff}^H &= \frac{\mu_{f+1} k_{f+1} (\partial \Im_{f+1} \hbar_{f+1} - \Im_{f+1} \partial \hbar_{f+1})}{\mu_f k_{f+1} \partial \Im_{f+1} \hbar_f - \mu_{f+1} k_f \Im_{f+1} \partial \hbar_f}, \\ T_{Pf}^V &= \frac{\mu_{f+1} k_{f+1} (\partial \Im_{f+1} \hbar_{f+1} - \Im_{f+1} \partial \hbar_{f+1})}{\mu_f k_{f+1} \partial \Im_f \hbar_{f+1} - \mu_{f+1} k_f \Im_f \partial \hbar_{f+1}}, \\ R_{Ff}^V &= \frac{\mu_f k_{f+1} \Im_{f+1} \partial \Im_f - \mu_{f+1} k_f \Im_f \partial \Im_{f+1}}{\mu_1 k_{f+1} \Im_{f+1} \partial \hbar_f - \mu_{f+1} k_f \partial \Im_{f+1} \hbar_f}, \\ R_{Pf}^H &= \frac{\mu_f k_{f+1} \partial \hbar_{f+1} \hbar_f - \mu_{f+1} k_f \hbar_{f+1} \partial \hbar_f}{\mu_f k_{f+1} \partial \hbar_{f+1} \Im_f - \mu_2 k_f \hbar_2 \partial \Im_f}, \\ T_{Ff}^V &= \frac{\mu_{f+1} k_{f+1} (\Im_{f+1} \partial \hbar_{f+1} - \partial \Im_{f+1} \hbar_{f+1})}{\mu_f k_{f+1} \Im_{f+1} \partial \hbar_f - \mu_{f+1} k_f \partial \Im_{f+1} \hbar_f}, \\ T_{Pf}^H &= \frac{\mu_{f+1} k_{f+1} (\partial \Im_{f+1} \hbar_{f+1} - \partial \Im_{f+1} \hbar_{f+1})}{\mu_f k_{f+1} \Im_f \partial \hbar_{f+1} - \mu_{f+1} k_f \partial \Im_f \hbar_{f+1}}, \\ R_{Ff}^H &= \frac{\mu_f k_{f+1} \partial \Im_{f+1} \Im_f - \mu_{f+1} k_f \partial \Im_{f+1} \Im_f}{\mu_f k_{f+1} \partial \Im_{f+1} \hbar_f - \mu_{f+1} k_f \Im_{f+1} \partial \hbar_f}, \\ R_{Pf}^V &= \frac{\mu_f k_{f+1} \partial \hbar_f \hbar_{f+1} - \mu_{f+1} k_f \hbar_f \partial \hbar_{f+1}}{\mu_f k_{f+1} \hbar_{f+1} \partial \Im_f - \mu_{f+1} k_f \partial \hbar_{f+1} \Im_f}, \end{aligned} \quad (\text{A27})$$

To simplify the complicated representation, the following parameters

$$\begin{aligned} \Im_f &= j_{\nu,f} (k_{tf} r_f) |_{\rho=k_{tf} r_f}, \\ \hbar_f &= h_n^{(1)} (k_{tf} r_f) |_{\rho=k_{tf} r_f}, \\ \partial \Im_f &= \frac{1}{\rho} \frac{d [\rho j_{\nu}(\rho)]}{d \rho} |_{\rho=k_{tf} r_f}, \\ \partial \hbar_f &= \frac{1}{\rho} \frac{d [\rho h_{\nu}^{(1)}(\rho)]}{d \rho} |_{\rho=k_{tf} r_f}, \end{aligned} \quad (\text{A28})$$

are used in Eq. (A27). From the boundary conditions (A25), we obtain two recurrence matrices relations. Solving the coupled matrix equations, after some manipulations, the unknown coefficients  $B_{M,N}^{11}$  are derived as

$$B_l^{11} = -\frac{T_{l,12}^1}{T_{l,11}^1}. \quad (\text{A29})$$



Here, the following matrix are also used to shorten the above expression

$$\begin{aligned} [T_l^K]_{2 \times 2} &= [T_{l,N-1}] [T_{l,N-2}] \cdots [T_{l,K+1}] [T_{l,K}] \\ &= \begin{bmatrix} T_{l,11}^K & T_{l,12}^K \\ T_{l,21}^K & T_{l,22}^K \end{bmatrix}. \end{aligned} \quad (\text{A30})$$

- 
- [1] J. B. Pendry, D. Schurig and D. R. Smith, *Science*, **312**, 1780 (2006).
  - [2] U. Leonhardt, *Science*, **312**, 1777 (2006).
  - [3] D. Schurig, J. J. Mock, B. J. Justice, S. A. Cummer, J. B. Pendry, A. F. Starr, and D. R. Smith, *Science* **314**, 977 (2006).
  - [4] J. B. Pendry, *Phys. Rev. Lett.* **85**, 3966 (2000).
  - [5] D. Schurig, J. B. Pendry, and D. R. Smith, *Opt. Express*, **15**, 14772 (2007).
  - [6] H. Y. Chen and C. T. Chan, *Appl. Phys. Lett.* **90**, 241105 (2007).
  - [7] E. E. Narimanova, and A. V. Kildisheva, *Appl. Phys. Lett.* **95**, 041106 (2009).
  - [8] D. A. Genov, S. Zhang and X. Zhang, *Nature Physics*. **5**, 687 (2009).
  - [9] H. Chen, R-X. Miao and M. Li, *Optics Express*. **18**, 15183 (2010).
  - [10] A. Greenleaf, Y. Kurylev, M. Lassas and G. Uhlmann, *Phys. Rev. Lett.* **99**, 183901 (2007).
  - [11] I.I. Smolyaninov, and Y.-J. Hung, *J. Opt. Soc. Am. B* **28**, 1591 (2011).
  - [12] I.I. Smolyaninov, Y.-J. Hung, and E. Hwang, *Phys. Lett. A* **376**, 2575 (2012).
  - [13] S. A. Cummer, B.-I. Popa, D. Schurig, D. R. Smith, and J. B. Pendry, *Phys. Rev. E* **74**, 036621 (2006).
  - [14] W. Cai, U. K. Chettiar, A. V. Kildishev, and V. M. Shalaev, *Nat. Photonics* **1**, 224 (2007).
  - [15] J. Li and J. B. Pendry, *Phys. Rev. Lett.* **101**, 203901 (2008).
  - [16] R. Liu, C. Ji, J. J. Mock, J. Y. Chin, T. J. Cui, and D. R. Smith, *Science* **323**, 366 (2009).
  - [17] H. F. Ma and T. J. Cui, *Nat. Commun.* p. 1:21 doi:10.1038/ncomms1023 (2010).
  - [18] J. Valentine, J. Li, T. Zentgraf, G. Bartal, and X. Zhang, *Nature Mater.* **8**, 568 (2009).
  - [19] J. H. Lee, J. Blair, V. A. Tamma, Q. Wu, S. J. Rhee, C. J. Summers, and W. Park, *Opt. Express* **17**, 12922 (2009).
  - [20] T. Ergin, N. Stenger, P. Brenner, J. B. Pendry, and M. Wegener, *Science* **328**, 337 (2010).
  - [21] X. Z. Chen, Y. Luo, J. J. Zhang, K. Jiang, J. B. Pendry and S. Zhang, *Nat. Commun.*, **2**, 176 (2011).
  - [22] B. L. Zhang, Y. Luo, X. G. Liu and G. Barbastathis, *Phys. Rev. Lett.* **106**, 033901 (2011).
  - [23] W. J. M. Kort-Kamp, F. S. S. Rosa, F. A. Pinheiro, and C. Farina, *Phys. Rev. A* **87**, 023837 (2013).
  - [24] F. Kheirandish, E. Amooghorban, *Phys. Rev. A*, **82**, 042901 (2010).
  - [25] F. Kheirandish, E. Amooghorban, and M. Soltani, *Phys. Rev. A*, **83**, 032507 (2011).
  - [26] E. Amooghorban, M. Wubs, N. Asger Mortensen, and F. Kheirandish, *Phys. Rev. A* **84**, 013806 (2011).
  - [27] E. Amooghorban and M. Wubs, submitted (2016).
  - [28] J. J. Hopfield, *Phys. Rev.* **112**, 1555 (1958).
  - [29] R. Matloob, R. Loudon, S. M. Barnett, and J. Jeffers, *Phys. Rev. A*, **52**, 4823 (1995).
  - [30] R. Matloob, *Phys. Rev. A*, **70**, 022108 (2004).
  - [31] L. Knöll, S. Scheel, and D.-G. Welsch, in *Coherence and Statistics of Photons and Atoms* (Wiley, New York, 2001)
  - [32] H. T. Dung, L. Knöll, and D.-G. Welsch, *Phys. Rev. A*, **62**, 053804 (2000).
  - [33] H. T. Dung, S. Y. Buhmann, L. Knöll, D. G. Welsch, S. Scheel, and J. Kästel, *Phys. Rev. A*, **68**, 043816 (2003).
  - [34] J. D. Jackson, *Classical electrodynamics* (Wiley, New York, 1999).
  - [35] C. T. Tai, *Dyadic Green functions in electromagnetic theory* (IEEE press, New York, 1994).
  - [36] L. W. Li, P. S. Kooi, M. S. Leong, and T. S. Yeo, *IEEE Trans. Microwave Theory Tech.* **42**, 2302 (1994).
  - [37] C.-W. Qiu, S. Zouhdi, and A. Razek, *IEEE Trans. Antennas Propag.* **55**, 3515 (2007).
  - [38] Y. Huang, Y. Feng, and T. Jiang, *Opt. Express*, **15**, 11133 (2007).
  - [39] C. W. Qiu, L. Hu, X. Xu, and Y. Feng, *Phys. Rev. E*, **79**, 047602 (2009).
  - [40] M. Brune, P. Nussenzveig, F. Schmidt-Kaler, F. Bernardot, A. Maali, J. M. Raimond, and S. Haroche, *Phys. Rev. Lett.* **72**, 3339 (1994).
  - [41] H. T. Dung, L. Knöll, and D. G. Welsch, *Phys. Rev. A* **64**, 013804 (2001).